Solid-state nuclear track detectors and their use in experimental nuclear physics

S. P. Tret'yakova
Joint Institute for Nuclear Research, Dubna

Fiz. Elem. Chastits At. Yadra **23**, 364–429 (March–April)

A brief review of the principles and methods of detection of heavy charged particles by solid-state nuclear track detectors is given. Topics covered include physicochemical aspects of the process of revealing tracks of ions by chemical etching, the choice of the optimum treatment regime to obtain a definite geometrical track shape, high detection efficiency, and controlled sensitivity of the solid-state nuclear track detectors to charged particles. The relationship between the parameters of the etched tracks and the ion energy and ionization, direction of motion, and angle of entry into the detector is established. Methods of identifying ions of various energies and charges are presented. An analysis is made of the spectrometric characteristics in a wide range of charges, energies, and masses of the particles, and the influence on them of high backgrounds of γ and α radiation, temperature, and oxygen in the air is also considered. The possibility of using the detectors in some nuclear-physics experiments is demonstrated for specific examples.

INTRODUCTION

Heavy-ion physics is one of the most rapidly developing fields of contemporary nuclear physics. Nuclear reactions initiated by heavy ions have given qualitatively new and sometimes unique possibilities in investigations into the mechanism of fusion of complex nuclear systems, the synthesis of new elements and isotopes, the study of radioactive decay of nuclides near the nucleon-stability limit, and in the development of many other directions of nuclear physics. At the same time, interactions of complex nuclei are characterized by many reaction channels, and this imposes severe requirements on the detection apparatus, which must be capable of detecting and identifying charged particles and fission fragments that are the products of nuclear reactions produced with small cross sections under complicated conditions with a high radiation background. Many different detectors and detecting facilities have been developed, but as yet universal detecting devices do not exist in low-energy heavy-ion physics. One of the directions of detector development made specially for heavy-ion physics is associated with solid-state nuclear track detectors (SSNTDs). The passage of heavy charged particles through most insulators leads to the formation, at the microstructural level, of narrow regions of radiation-damaged matter—latent tracks.[1] In crystals, such a track can be detected by means of an electron microscope, and in polymers by means of special coloring of the radiation-damaged material.[2] However, these methods are too laborious and impracticable for seeking and studying of rare events in the large areas of the detectors usually employed in nuclear-physics experiments. For these purposes, it is better to use an optical microscope after appropriate etching of the irradiated material. In 1958, Young[3] first succeeded in detecting the effect of selective etching of the tracks of fragments from the fission of ^{235}U nuclei by thermal neutrons in lithium chloride crystals; in 1959, Silk and Barnes, using an electron microscope, discovered fission-fragment tracks in thin layers of muscovite mica, which disappeared during observation under the microscope.[1] At the beginning of the sixties, Price and Walker[4] proposed that the traces of the charged particles in mica and polymer should be preserved by selective etching of the damaged material along the particle trajectories.

The establishment of a relationship between the rate of etching of material along the track of an ion and its ionization losses stimulated the development of methods of identifying the charge, mass, energy, and orientation of particles. The creation of the method based on SSNTDs was also fostered by the experimental testing of various models of the formation of latent and etched tracks of charged particles in different materials, the development of instrumental methods for investigating the physical and chemical interactions of charged particles with matter, and the development of new polymer and inorganic materials.

In the first part, we briefly review the data on the formation and nature of the latent tracks of heavy charged particles in insulators. We present data on the process of chemical treatment that permit the optimum regime for revealing and enhancing the latent tracks in various materials, calibrated under various conditions by accelerated ions. Further, we consider aspects of the detection efficiency and sensitivity, and also the possibility of controlling the sensitivity threshold of the detectors under various conditions of physics experiments. We present some methods of identifying heavy ions and the spectrometric characteristics of SSNTDs in a wide range of charges, energies, and masses, and we also consider the effect on them of high γ and α radiation, ambient temperature, and oxygen present in it. Finally, as an illustration of the method, we demonstrate the use of SSNTDs in some physics experiments to detect products of radioactive decay and heavy-ion nuclear reactions.

 0090-4759/92/020156-31$04.00

1. THE NATURE OF LATENT CHARGED-PARTICLE TRACKS AND THEIR ENHANCEMENT BY ETCHING

Transfer of heavy-ion energy to solids

From the point of view of energy loss, three main types of heavy-ion interaction with matter can be distinguished:[5] 1) interaction of the nucleus of the ion with the electron shells of the matter; 2) interaction of the electrons of the ion with the nuclei of the atoms of the material; 3) interaction of the nucleus of the ion with the atoms of the matter. The contributions of these processes to the energy loss are mainly determined by the ion velocity. The description of the specific energy losses for all heavy-ion energies is complicated because the ion charge (the most sensitive interaction characteristic) changes as the ion moves in the matter (until it stops). The dependences of the specific energy losses on these ion parameters is complicated and cannot be represented by a single analytic expression. Usually, one distinguishes ranges of ion velocities in each of which one of the above processes of ion interaction with the atoms of the matter is predominant. A detailed description of these processes can be found in Ref. 5.

The total energy losses rates can be represented in the form

$$(dE/dx)_{\text{tot}}=(dE/dx)_{\text{nu}}+(dE/dx)_{\text{el}},$$

where the terms on the right-hand side of the equation correspond to the nuclear and electron interactions, respectively. Lindhard *et al.*[6] studied the stopping of ions and estimated the fraction of the energy lost as a result of atomic and electron deceleration. The nucleon component is dominant at low ion energies (below 0.01 MeV/amu); above 0.1 MeV/amu, the electron component increases as $\sqrt{E}$ (where E is the ion energy), reaching a maximum, depending on the ion species, between 1 and 10 MeV/amu, and then decreasing as $1/E$ with increasing energy.[5]

The ion energy is transferred to the medium mainly either by ionization of atoms in the immediate vicinity of the trajectory by the ion itself or by energetic electrons that are knocked out along the trajectory and ionize the medium at some distance, at times appreciable, from the ion trajectory. Knowledge of the energy losses responsible for the etchability of the nuclear tracks is needed in almost all fields in which SSNTDs are used. The total energy losses can be calculated using the Bethe–Bloch formula.[7–9]

The electrons knocked out by the incident ion have a broad spectrum of kinetic energies with a clear maximum at low energies (a consequence of the behavior of the Rutherford scattering cross section) not exceeding the ionization energy. A small fraction of collisions give rise to electrons with high energy, which, in their turn, can create a volume ionization density. Detailed calculations of the energy deposition near an ion track were made in Refs. 10–12. It was found in Refs. 10 and 11 that most of the energy of the δ electrons is deposited a few nanometers from the ion track. For fast ions, approximately half the energy is carried away by the δ electrons, and from the remaining energy loss about half becomes excitation energy of electrons in atoms; about 25% of the total energy loss is expended on overcoming the ionization potential of the atoms of the target material.[12]

It was shown experimentally[8] that the secondary effects associated with the δ electrons do not play a significant role in the formation of the latent tracks in inorganic SSNTDs (crystals, glasses). In them, the radiation damage in the region of a latent track is done mainly by the primary ionization I, which is determined from the relation[7]

$$I=CZ_{\text{eff}}^2/\beta^2[\ln(\beta^2/(1-\beta^2))-\beta^2-\delta+k], \quad (1)$$

where Z_{eff} is the effective charge of the particle,

$$Z_{\text{eff}}=Z_1[1-\exp(-130\beta/Z_1^{2/3})], \quad (2)$$

$\beta=v/c$, and c is the speed of light.

In Eq. (1), C and k are constants for a given stopping medium, and δ is a relativistic correction associated with the polarization of the medium. The value of k is chosen empirically[8] and used as a correction parameter, and I is calculated in arbitrary units.

In polymers, in contrast, secondary ionization and excitation can damage the material structure,[11,13] but the total energy loss dE/dx cannot be used as a criterion for track identification.[9] The concept of restricted energy loss (REL), taking into account the particle–matter interaction, was proposed in Refs. 13 and 14. The total energy loss dE/dx can be represented as a sum of two components:

$$dE/dx=(dE/dx)_{\omega>\omega_0}+(dE/dx)_{\omega<\omega_0}, \quad (3)$$

where $(dE/dx)_{\omega>\omega_0}$ is the energy loss in near interactions, in which electrons with energy $\omega>\omega_0$ are knocked out, and $(dE/dx)_{\omega<\omega_0}$ is the energy loss in distant interactions, for which $\omega<\omega_0$.

The parameter ω_0 (electron energy) is chosen in such a way that for near interactions the electrons of the atoms can be treated as free particles, and for distant interactions as point charges. Thus, the parameter ω_0 determines the boundary between the electrons that are and are not taken into account in the track formation. The components can be represented in the form

$$(dE/dx)_{\omega>\omega_0}=C_1Z_{\text{eff}}^2\beta^{-2}[\ln(\omega_{\max}/\omega_0)-\beta^2], \quad (4)$$

$$(dE/dx)_{\omega<\omega_0}=C_1Z_{\text{eff}}^2\beta^{-2}[\ln(\omega_{\max}\omega_0/\bar{I}_a^{-2})-\delta-U], \quad (5)$$

where $\omega_{\max}$ is the maximum energy transfer, determined by $\omega_{\max}=4M_1M_2E/(M_1+M_2)$; $\bar{I}_a$ is the mean ionization potential of the atomic electrons of the stopping medium; U is a term that takes into account the properties of the interaction with electrons in inner shells; $(dE/dx)_{\omega<\omega_0}$ is used to calculate the energy left near the track in the case of distant collisions and is called the REL.

If the stopping power is known along the complete path of the ion in the matter, then its mean total range is given by

$$\bar{R}(E)=\int_0^E (dE/dx)^{-1}dx. \quad (6)$$

The electron stopping power can be fairly well calculated; the nuclear analog is much less well known. This introduces an uncertainty in calculations of the mean total range. Usually, the ion range in the matter is calculated on the basis of the semiempirical model proposed in Ref. 13. In this case, the range R of a charged particle with given velocity $v=c\beta$ in the matter is determined by the expression

$$R(\beta)=MZ^{-2}[\lambda(\beta)+B_Z(\beta)], \tag{7}$$

where M and Z are the mass and charge of the particle; $\lambda(\beta)$ is the range of an "ideal" proton with velocity $c\beta$ without neutralization of the charge near the stopping at the end of the track; and $B_Z(\beta)$ is a generalized increase of the range due to neutralization of the charge of the moving ion near the end of the track.

Calculations of $dE/dx(E)$ and $R(E)$ for heavy ions in various media were published in Refs. 15–19. Corrections for nuclear interactions are made in Ref. 16. For polymers used as SSNTDs, REL model calculations are given in Refs. 15, 17, and 18. It is expedient to use the tabulated data of Refs. 15 and 17 for ion energies greater than 1 MeV/amu; at lower energies, the experimental data do not agree with the calculations. In reality, it is better to determine the range–energy dependence for each material experimentally.

In some studies,[10–12] the spatial distribution of the absorbed energy in insulators after passage of an ion has been calculated. Comparison with experimental data shows that the radial distribution $D(r)$ of the absorbed dose in polymers can be described in a first approximation by the relation

$$D(r)\sim 1/r^2. \tag{8}$$

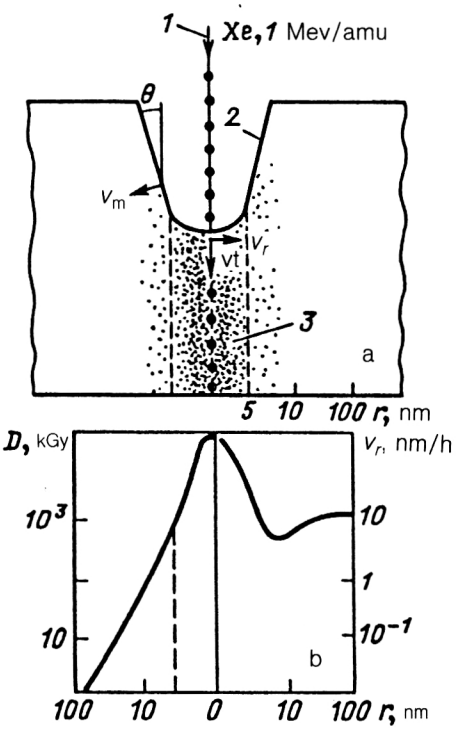

FIG. 1. Schematic model of etching of xenon track: a) formation of track; 1) direction of motion of ion; 2) etching front; 3) region of radiation damage of material. The points show the density of radiation defects; the broken line bounds the region of the latent track, where the radial etching velocity v_r of the track region is greater than the etching velocity v_m of the detector material; v_t is the etching velocity of the material in the region of the ion track along its trajectory; θ is the cone angle; b) change of the absorbed dose D (on the left) and the radial velocity v_r (on the right) with increasing distance r from the ion trajectory.

Nature, structure, and formation mechanisms of etched tracks in SSNTDs

Investigations of latent tracks by means of electron microscopes and selective etching showed that tracks are formed in solids with resistivity not lower than $\sim 2\cdot 10^3$ $\Omega\cdot$cm.[8] Some data on the nature, size, and structure of latent tracks were obtained by various physicochemical methods: by electron microscopes,[1,20–23] small-angle neutron scattering and x-ray radiation,[24,25] ultraviolet and infrared spectroscopy,[26,27] spectrometry, electron spin resonance,[28,29] thermoluminescence,[30] the conductance-measurement method,[31–34] track annealing,[35–38] and sputtering of matter by heavy ions.[39] It follows from analysis of these data that as a heavy ion moves along its trajectory in an insulator it creates a narrow (a few nanometers wide) region of damaged material with a lowered density and an enhanced etchability of the material compared with its surroundings. To illustrate the track size and etchability in relation to the absorbed dose (see the calculation of Ref. 19), Fig. 1 shows the results[34] of a measurement of the radial etching rate v_r of a xenon track ($E\sim 1$ MeV/amu) obtained by the conductance-measurement method of etching of a thin (about 2.5 μm) layer of an SSNTD made of polyethylene terephthalate (PETP). It can be seen that v_r is maximal in a relatively narrow interval of doses near the track center. The decrease of v_r along the track radius is due to the decrease in the absorbed dose. The complicated form of the curve indicates that there are different radiochemical processes in the track region. At a dose less than $5\cdot 10^2$ kGy, the material of the track zone at radius greater than 7 nm no longer exhibits enhanced etchability. The sharp rise of v_r in Fig. 1 in a relatively narrow interval of doses indicates the threshold nature of the detector sensitivity.

For track formation, quite a long time is required, during which various physicochemical processes that ensure the stability of the formed material structure of the track take place in its region.[14] Appreciable differences are observed in the extension and type of defects produced by ions in inorganic (crystals and glasses) and organic (polymer) insulators.[8]

Among the many models of track formation in insulators so far proposed, we must mention the semiquantitative notion of the *ion explosion spike*.[8,40–43] This explains most fully the formation of latent tracks of ions in inorganic materials.[42] It is assumed that as the particle interacts with matter along its trajectory there is formed a zone of ionized atoms, which, owing to the Coulomb interaction, pass from the inner to the outer zone, creating an extended zone of

structure defects of the insulator. According to Ref. 43, there is a two-zone structure of the forming region of radiation damage. A narrow cylindrical zone (zone radius of order 1.0 nm) along the track axis is enriched with vacancies, while the region with radius r is filled with atoms displaced from the central region. If a track is to form, the forces of the Coulomb interaction of the ionized atoms must appreciably exceed the lattice binding forces. Using parameters like the lattice constant, permittivity, and Young modulus, this model makes it possible to predict the relative sensitivity of insulators with respect to particles and to show why tracks are not detected in good semiconductors and metals.

In ion-detecting polymers, material is destroyed under the influence of ionization. Electrons and ionized and excited molecules are formed and can interact and recombine, forming free radicals and stable molecules. It was shown in Ref. 44 that the formation of tracks in polymers is correlated with the molecular-chain breaking number G (the number of chain breaks per 100 eV of expended energy). It is probably this process, which results from excitation of electrons, that is mainly responsible for the track formation in polymers.[40] In the region of the track, a large number of broken molecular chains is formed, leading to a decrease of the molecular mass of the matter and an increase of its etching rate. In this case, the sensitivity threshold of the insulator can be related to the formation of the necessary number of broken bonds in the polymer resulting from passage of a particle and determined as a function of the absorbed dose.[44,45]

It follows from analysis of the available data on the formation of etchable latent tracks in insulators that the complicated process of energy loss of a heavy charged particle in matter makes it difficult to establish a unique relationship between its ionization and the parameters of the etched region of the latent track. The models of this process hitherto used are very restricted, as regards both the set of ions and the properties of the detector material. However, it is extremely important to understand what mechanisms of energy transfer to the matter are important for the formation of an etchable latent track. All the existing models assume that etchable damage made by an ion in a detector can be described by a quantity of the type dE/dx. In each model, there are free parameters chosen to achieve the best description of the experimental data. Therefore, the particular numerical values of the free parameters apply only to the materials and conditions of track development under which they were obtained. If there are any changes, it is necessary to make new calibrations and appropriate calculations.

From the point of view of agreement with experiment, the most realistic models have been found to be the primary-ionization model,[8] the model of restricted energy loss (REL model),[13] and the model of minimum ionization density in the volume of a track fixed by a certain distance of about 2 nm from the ion trajectory.[10,46] For inorganic SSNTDs, the best agreement with the experimental data is obtained with the primary-ionization model [see Eq. (1)],[87] and for polymers with the REL model.[13] In the first case, it is assumed that only primary ionization and excitation events give rise to chemically active defects, which determine the enhanced etching rate, and a track is revealed only when the linear ionization density produced along the trajectory of the primary particle exceeds a certain critical value for the given material (sensitivity threshold).[10] In the REL model, the decisive parameter has been chosen to be the fraction of the energy loss due to collisions in which an energy less than a certain value is transferred [see (5)]. The semiempirical model of minimum ionization density,[10,46] assumes that an etchable track arises only when the absorbed dose produced by the secondary electrons in a volume bounded by the fixed distance 2 nm from the track trajectory exceeds a certain threshold value. In subsequent work, the authors of Ref. 12 took into account both primary and secondary ionization processes in calculations of the radial distribution of the absorbed dose in polymers and showed that in the track center a large fraction of the energy is expended on primary processes.

In Refs. 8 and 33, various models were analyzed, their shortcomings were noted, and some general conclusions were drawn. Although the given criteria require careful experimental verification for different forms of detectors and energy ranges, they do make it possible to compare different calibration data and to classify materials according to their sensitivity threshold.

The sensitivity threshold is characterized by a definite minimum ionization density (critical energy loss) above which a track can be revealed by etching, or by a maximum energy below which the track of an ion that enters the detector at right angles will be revealed by etching. Table I gives the threshold sensitivities (with respect to the ion energy) of some of the SSNTDs most often used in physics experiments,[8] and in Fig. 2 the horizontal lines show the relative sensitivity thresholds (in ionization energy losses) of SSNTDs obtained experimentally in Ref. 47 above which the represented ions form tracks with 100% efficiency. It can be seen that the different detector types differ strongly in sensitivity, so that, depending on the requirements of the experiment, one can choose a detector (or several different types of detector) with appropriate threshold sensitivity. It should be noted that the threshold energy can vary appreciably, depending on the properties of the detector material, the conditions of use, and the treatment regimes. This necessitates continual calibration under conditions close to those of the experiment.

Physicochemical properties of SSNTDs

Industry produces practically no special materials for charged-particle detection. Therefore, plastic, glass, and minerals intended for other purposes are generally used as SSNTDs. Moreover, the composition of the polymers can change from batch to batch and with time, especially if they contain a volatile component. The amount of oxides in glasses is not rigorously controlled, and the composition of minerals is not constant. In connection with the commissioning of accelerators of multiply charged particles, there is active study of radiochemical processes in materi-

TABLE I. Relative threshold sensitivity of the polyethylene terephthalates most often used in physics experiments.[8]

Type of detector*	Chemical composition	Energy, MeV, and species of ion whose tracks are detected
	Inorganic insulator	
Olivine	$MgFeSiO_4$	100; ^{56}Fe
Quartz	SiO_2	100; ^{40}Ar
Muscovite mica (MM)	$KAl_3Si_3O_{10}(OH)_2$	2; ^{20}Ne
Phlogopite mica (PM)	$KMg_2Al_2Si_3O_{10}(OH)_2$	2; ^{20}Ne
Quartz glass	SiO_2	2; ^{20}Ne
Na–Ca	$23SiO_2:5Na_2O:5CaO:Al_2O_3$	20; ^{20}Ne
phosphate (PG)	$10P_2O_5:1,6BaO:Ag_2O:2K_2O:2Al_2O_3$	20; ^{20}Ne
	Organic insulator	
Polyethylene terephthalate (PETP)	$C_5H_4O_2$	12; ^{12}C
Polycarbonate (PC)	$C_{16}H_{14}O_3$	0,3; ^4He
Cellulose nitrate (CN)	$C_6H_8O_9N_2$	0,55; ^1H
Poly-allyl-glycol -carbonate (PAGC)	$C_{12}H_{18}O_7$	100; ^4He

*The names and addresses of the firms supplying these materials can be found in Refs. 8 and 38.

als exposed to a high ionization density resulting from the passage of ions through the matter. Some spectral characteristics of the damaged material of tracks resulting from irradiation of PETP, PC, and PAGC with different ion beams have been obtained;[47–52] studies have been made of the products of radiolysis in some SSNTDs (Refs. 26–29, 53, and 54), and also of parametric centers for various doses, temperatures, and time after irradiation.[55]

Polymers for which the ionization damage appreciably exceeds the amount of cross-linking are used as detectors.[14,48,49] Breaks of molecules lead to the formation of shorter molecules with higher reactivity. The presence of oxygen fosters the damage process. The influence of the degree of polymerization, nitration, plastification, orientation, and distribution of the molecular mass on the detection properties of various polymers was studied in Refs. 13, 47, and 56–61. It was found that the track shape is improved with increasing molecular mass. This led to a lower energy spread of the investigated particles (Refs. 13, 47, 56, and 57). The properties of the detectors also change with the crystallinity. For amorphous PETP, the sensitivity threshold is higher.[28] Complete crystallization of PETP improves its properties.[28,58,59] The different behaviors of the crystalline and amorphous phases must be taken into account when polymers with partial crystallization are used, for example, PETP for which the crystallinity is about 40%.[55,58] In the case of cellulose nitrate, the experiment showed that it is expedient to use materials with higher nitration, polymerization, and a narrow distribution of the molecular mass. The greatest sensitivity is observed when camphor and dibutyl phthalate are used as plasticizers.[57–59] Poly-allyl-glycol-carbonate (PAGC) needs to be prepared under a strictly controlled thermal regime.[62,63] The pure polymer has the greatest sensitivity.[64]

Among amorphous inorganic materials, silicate, phosphate, and quartz glasses are used. Prescriptions for preparing phosphate glasses are given in Refs. 65–67. Industrial samples of silicate and quartz glasses are used. Depending on their structure, crystals (mica, olivine, etc.) possess isotropy of their properties.[47,68] This affects the etching process, track shape, and detection efficiency of the detectors. The etching rates and track lengths along different crystal planes can differ strongly.[47,69] For example, the ion range in muscovite mica can, depending on the angle of entry and the azimuth, vary by up to 19%.[47,70,71] Table II gives the properties of some insulators most often used as detectors in physics experiments.

Calibration of detectors

The radiation properties of potential materials are investigated by means of accelerators, radionuclide sources of α particles and fragments, nuclear reactors, microtrons, and γ sources. Calibration is needed not only to study new materials but also for known materials, for which the properties can change with time (aging). The detector is irradiated with ion beams with different but known E, M, Z. There now exist numerous accelerators of multiply charged ions that provide a wide spectrum of ions, both in charge (up to uranium) and in energy. As a rule, the detectors are irradiated in special devices that ensure the required angle of entry into the detector, flux, and energy of the ions. One of the most automated constructions is described in Ref. 72. In calibration experiments with exact

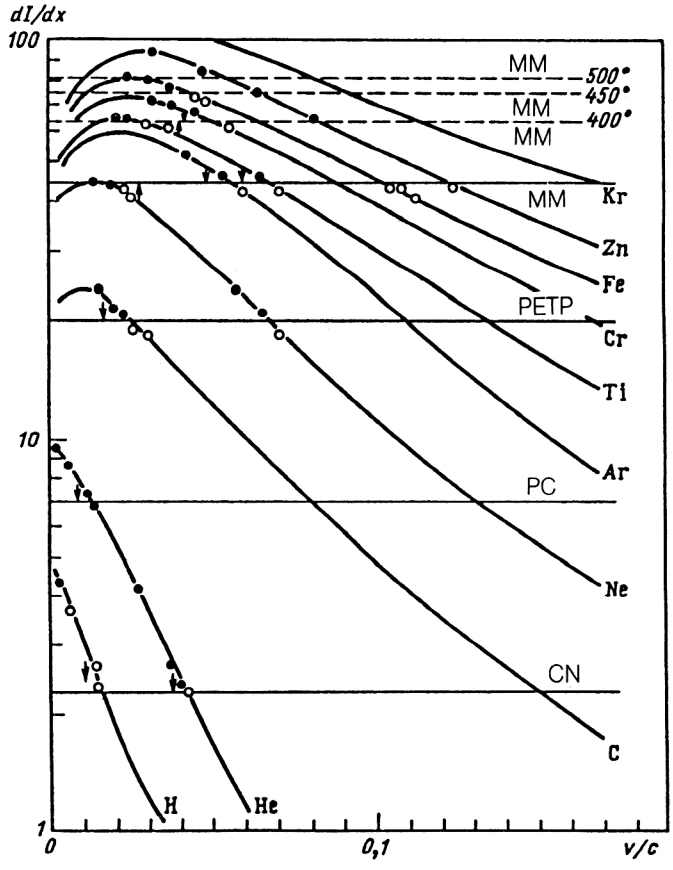

FIG. 2. Damage intensity (in relative units of the primary energy loss dI/dx) as a function of the relative velocity of various ions.[8] The horizontal lines and arrows indicate the sensitivity thresholds of the various SSNTDs (Table I); the broken lines are the changes in the sensitivity thresholds as a result of annealing of muscovite mica at the temperatures 400, 450, and 500 °C;[47] the black circles indicate observation of tracks; the open circles indicate absence of their detection.

knowledge of the energy of the beam of ions incident on the detector and the dispersion of the energy, use is made of a facility with a large scattering chamber, with magnetic analysis of the beam of charged particles leaving the chamber, or the focal plane of a magnetic spectrometer with adjustment controlled by a semiconductor telescope.[73–75]

As a rule, the sources of fission fragments and α particles are natural radioactive preparations of various activities: ^{235,238}U, ^{238,239}Pu, ^{241}Am, ^{252}Cm. To determine the fissioning isotopes present as impurities (uranium, thorium) in detectors, reactor neutrons and microtrons are used.[8,76] The sensitivity to γ rays is investigated by means of ^{137}Cs and ^{60}Co preparations, and also microtrons.[76] Ultraviolet sensitizing is done by means of ultraviolet lamps.[22,77]

Chemical etching to develop and enhance latent tracks

The general scheme of obtaining an etchable track is shown in Fig. 3. For each stage, this gives the main parameters that determine the formation, development, and enhancement of the track. In the case of etching by means of selected chemical reactants by means of oxidation (HF, $KMnO_4$, H_3PO_4, etc.) or alkali hydrolysis (NaOH, KOH), the material of the track zone and, partly, the detector is transformed into salts that dissolve in water. In the region of the particle trajectory, a hollow channel, which preserves the orientation and length of the latent track but which has a much larger diameter, is formed. Table III gives details of some of the most common etchants. The fullest list of prescriptions and solutions for various types of materials is given in Ref. 8.

The etching process has not been sufficiently studied. Mainly, it takes place from the surface, most probably in a monomolecular layer at the detector–solution interface.[58] It is assumed that the selectivity of the etching of the track zone is due to its enhanced chemical activity and to the presence of free space in this zone, which can be created by radiolysis of the material and removal of the gaseous phase. The kinetics of the etching process is investigated either through the change of the optically visible track parameters (electron microscopes are sometimes used) or by the method based on measurement of the conductance,[31–33] which makes it possible to determine the radial and longitudinal track etching rates in thin film materials. The construction of the apparatus and the method itself are described in Refs. 32 and 33.

The development of a track by etching can be represented as the result of two processes that take place practically simultaneously—etching of the detector material at a rate v_m and etching of the material in the region of the track at rate v_t. The first is determined from the ratio h/t, where h is the thickness of the etched layer and t is the etching duration,[78,79] while v_t is determined from the relation $v_t = L/t$, where L is the track length etched during time t. In the general case, v_t is a function of the coordinate of the point on the track axis. The selectivity of the track

TABLE II. Properties of insulators.

Material	Density, g/cm^3	Crystallinity, %	Melting point, °C
Muscovite mica	2,76—3,10	Crystal	700
Phosphate glass	2,9	Amorphous	500
Polyethylene terephthalate	1,39—1,41	55	250
Polycarbonate	1,2—1,3	Amorphous	250
Cellulose nitrate	1,40—1,52	70	200
Poly-allyl-glycol-carbonate	1,31	Amorphous	300

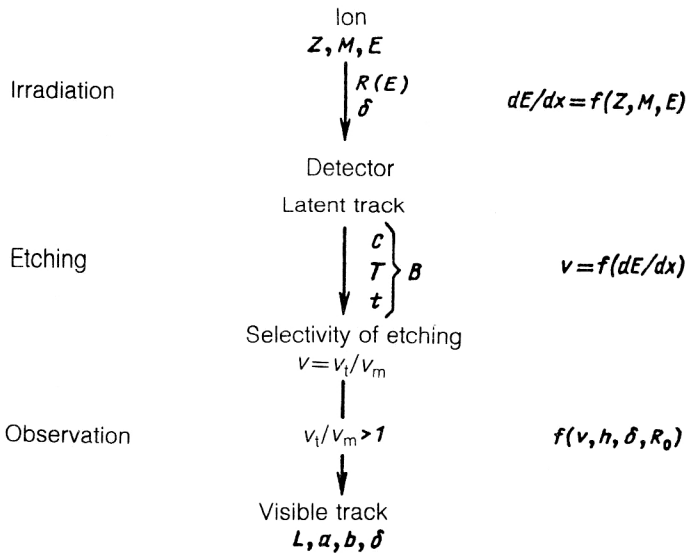

FIG. 3. Development of etchable track of an ion in a detector. The notation is as follows: dE/dx, Z, M, E, R, and δ are the rate of energy loss, the charge, the mass, energy, range, and angle of entry of the particle into the detector; C and T are the concentration and temperature of the solution for etching; h is the thickness of the etched layer of the detector during the etching time t, and L is the etched track length; a and b are the semimajor and semiminor axes of the entrance opening of the track channel.

etching process is characterized by the relative etching rate $v=v_t/v_m$ at the given point of the track and determines the geometrical shape of the track. The boundary condition for formation of a track that enters the detector at an angle (Fig. 4) has the form $L\sin\delta=h$. It follows that $(v_t/v_m)\sin\delta=1$. A track is developed if the angle of entry satisfies $\delta>\delta_{cr}$, where $\delta_{cr}=\arcsin(v_t/v_m)$. The etching rate depends on the temperature, the concentration of the etching solution, and the duration of the process.

As an example, Fig. 5 gives the etching rates of Ar and Xe in PETP as functions of the concentration and temperature, obtained by means of the conductance-measurement etching method.[47] For the etching, one chooses in the first place an etchant concentration for which variation of which has little effect on the etching rate; secondly, one chooses the range of temperatures in which one observes the best ion discrimination. There is a detailed description of the properties of the etching processes for various types of materials, depending on the concentration, temperature, and etching duration, in Refs. 56, 58, 72, and 80–84.

If v_m is determined by the detector properties and by the activity of the etching solution, v_m and v are also determined by the parameters of the particles and by the conditions under which the detectors are used (irradiation and use at a later time). As a rule, it is not possible to obtain an analytic dependence on the complete set of factors. Therefore, one usually finds an empirical expression for the dependence of v_t and v on the particle parameters for definite conditions of track development.

Determination of the parameters of an etched track

The track geometry in a given detector is basically determined by the etching selectivity, the isotropy of the medium, and the duration and kinetics of the etching process. Many studies have been devoted to the track geometry, among which we may distinguish Refs. 8, 13, and 85–88.

Depending on the etching time, three phases can be distinguished in the evolution of the geometrical shape of a track in glass and polymers: conical (1), transitional (rounded) (2), and spherical (3) (Fig. 6). The characteristic shapes of tracks of ions having different parameters are used for visual identification. The direction of motion

TABLE III. Determination of fission-fragment detection efficiency in 2π geometry for some detectors.[47]

Detector	Treatment	Efficiency of 2π detection, %	δ_{cr}, deg
Muscovite mica	40% HF, 22 °C, 120 min	90 ± 3	6
Flurophlogopite	20% HF, 20 °C, 10 min	83 ± 5	9,8
Phosphate glass	40% HF, 20 °C, 90 min	90 ± 3	6
PETP	20% NaOH, 60 °C, 60 min	95 ± 3	4
PETP	30% KOH, 70 °C, 60 min 1 kHz, 10 kV/cm	70 – 64	12 – 15
PC	20% NaOH, 70 °C, 60 min	95 ± 3	4
CN	10% NaOH, 40 °C, 60 min	90 ± 3	6
PAGC	20% NaOH, 70 °C, 60 min	90 ± 3	6

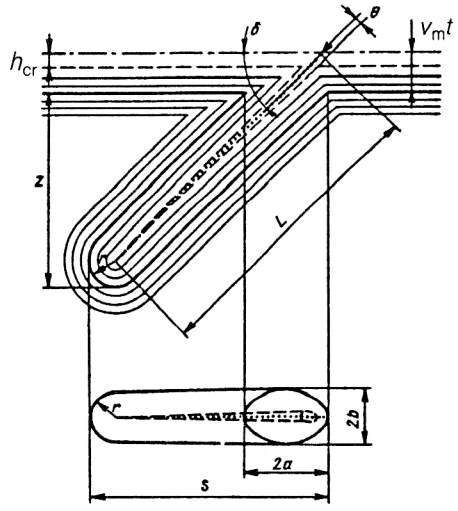

FIG. 4. Schematic representation of the change of the track shape with etching time (etched layer $h=v_m t$) in an isotropic detector.

and angle of entry of the ion into the detector are also reflected in the track shape. As an illustration, Fig. 7 shows microphotographs of the entrance openings of the track of a lithium ion that passed through a PAGC film, shown from opposite sides of the film.

The ratio v_t/v_m determines δ_{cr}, which, in its turn, determines not only the detection efficiency but also the track shape. Figure 8 shows microphotographs of tracks of ions that entered different detectors at different angles.

The selectivity of the track etching increases with increasing specific energy loss. This can be clearly seen in Fig. 8, which shows tracks of Zn and S with different dE/dx $[(dE/dx)_{Zn} > (dE/dx)_S]$.

When an ion passes through a detector, the degree of ionization changes continuously along its trajectory. A generalized geometrical model of etch-pit formation was developed in Ref. 88 with allowance for the change of v_t along the particle track. From a knowledge of the particle parameters and the dependence of v on the residual range R_{res}, this model enables one to calculate the parameters of the etched track and its profile. However, the calculation is rather complicated, and the agreement with the experimental data depends to a large degree on the uniformity of the properties of the detector and on the conditions of its use. For a small and steady change of the rate of ionization energy loss within the thickness of the detector (or during the investigated time interval), it is possible to use the formula for $v=\text{const}$ in a detector with isotropic properties (glasses and polymers).[85–87] In this case, the track parameters are measured at definite intervals of time during the etching of the detector material.

Analysis of the geometrical shape of the tracks in the conical and transitional etching phases in Refs. 85 and 86 yielded expressions for determination of the etched length L and the angle of entry δ of the ion into the detector for different sets of track parameters and varied intervals of angles. We give here the most frequently used expressions for calculation of the etched track length and angle of entry into the detector (see Fig. 4):

I. $10<\delta<45°$:

$$L=(S-r-h\,\mathrm{tg}[(\delta-\theta)/2])/\cos\theta,$$

$$\sin\theta=(h-r)/L,$$

$$\sin\delta=[a^2\sin^2\theta+b^2\cos^2\theta]^{1/2}/a,$$

$$\mathrm{tg}\,\theta=\left[\frac{(a^2-b^2)^{1/2}}{a}\right]\times\frac{[b^2(S-r-a)^2-(a^2-b^2)(b^2-r^2)]^{1/2}-r(S-r-a)}{(S-r-a)^2-(a^2-b^2)},$$

where S is the projection of the track length onto the plane; a and b are the semimajor and semiminor axes of the entrance opening of the track channel; $h=v_m t$ is the thickness of the etched layer; r is the radius of the rounded end of the track.

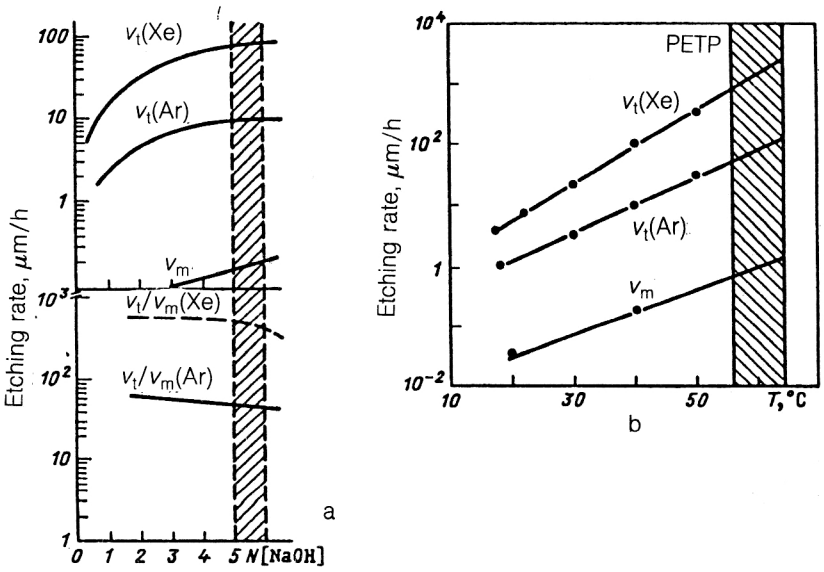

FIG. 5. Dependence of etching rate on the concentration of the etching solution (a) and its temperature (b) in NaOH solution for tracks of Xe and Ar ions entering a 6-μm film of PETP with energies 120 and 220 MeV, respectively.

FIG. 6. Microphotographs of conical (1), transitional (2), and spherical (3) shapes of tracks of ^{7}Li ions. In (2) one can see light shallow tracks of ^{4}He, for which v_t/v_m is smaller than for ^{7}Li tracks.

II. $20<\delta<75°$:

$$L=(z+h)/\sin\delta,$$

$$\sin(\delta-\theta)$$

$$=[r(S-r)+z(S^2-2Sr+z^2)^{1/2}]/[(S-r)^2+z^2],$$

$$\sin\delta/\sin\theta=(h+z)/(h-r),$$

$$\sin\theta/\sin\delta=C=[b(z^2+b^2-r^2)^{1/2}-zr]/(z^2+b^2),$$

where z is the track depth. In the case of an incompletely etched track (conical phase), we have the parameter $r=0$. Near the sensitivity threshold for small values of the selectivity, it is difficult to measure the track parameters, and the errors of measurement reach 100%. Therefore, for $v\leqslant 3$ the etched length and v are determined from the diameters D of the tracks of ions that enter the detector at 90°:[86]

$$v=\frac{(1+D^2/h^2)}{(1-D^2/h^2)},$$

where D is the diameter of the ion track, and h is the thickness of the layer etched during the etching time, from which $L=vh$. The error in the determination of L of an individual track is ± 0.3 μm.

In crystals, the tracks have a definite geometrical shape, which reflects the anisotropy of the chemical etching of these detectors with ordered crystalline structure. The etching rates and track parameters for crystalline SSNTDs are given in Ref. 86.

Methods of observation, counting, and measurement of track parameters

The experimentalists now have at their disposal a fairly large arsenal of methods and means for observing, determining the number, and measuring the parameters of charged-particle tracks. An optical microscope is most often used. It enables one to look for events, count them, and measure the track parameters. For scanning one usually employs a magnification of $\sim\times 100$ (scanning rate ~ 10 cm^2/h); for measurement of the track parameters one uses $\sim\times 1500$ (resolution down to 0.2 nm), for which the track density must not exceed $\sim 10^5$ cm^{-2}.

FIG. 7. Microphotographs of track of a lithium ion from opposite sides of a detector film (PAGC) through which the particle passed: a) the direction of advance of the etching is the same as the direction of motion of the ion; b) opposite directions.

For study of the etching kinetics in the early stage of the process, track counting at densities $\sim 10^6$ cm^{-2}, measurement of track sizes by the replica method,[90] and examination of the structure of the etched surface, use is made of electron microscopes, which ensure high spatial resolution in the transmission (down to 0.2–1.5 nm) and scanning models (down to 5–20 nm).

To find rare events, one employs various methods that increase the track size and establish its position. A very promising method in this connection is electrochemical etching,[38,90–93] which makes it possible to enlarge tracks to 100–150 μm and observe them visually or with a small magnification, using for this purpose photometers and microdensitometers.[94–96] In other cases, one works with a film of the detector whose thickness is less than the etchable track length. On etching, a track channel that passes right through the film is obtained, and to determine its position special coverings (paper, emulsion, aluminum film, etc.), which are applied (or deposited) on one side of the film, are used. The region of such a "right-through" track is colored by an indicator or dissolved by one-sided etching,[8,97] forming visible pits. The admissible density of tracks depends on the size of the visually observable pits then obtained and is in the range 10^{-2}–10^3 cm^{-2}. The detection of such pits can be automated.[38] In addition, such tracks in thin detectors can also be counted by means of spark or conductance-measurement methods.[38,98–101] In the first case, the thin detector with etched right-through tracks is placed on an electrode and covered with a thin aluminized polymer film or aluminum foil with thickness of about 5 μm, which is also an electrode. A voltage (about 500–800 V) is applied to the electrodes. A jumping spark evaporates the aluminum of the polymer film in the region of the track opening. The number of tracks can be determined automatically from the number of sparks in a few seconds. The Al replica reveals the distribution of tracks in the detector. The maximum measured density in the employed spark counters does not exceed $3\cdot 10^3$ cm^{-2}. In Ref. 102, the use of an additional mask demonstrated the possibility of measuring track densities up to $5\cdot 10^4$ cm^{-2}. The conductance-measurement method makes it possible to determine track densities 10^6–10^8 cm^{-2} in the case of the formation of right-through pores during etching in an electrolytic cell.[33]

Besides these methods, automatic systems of data analysis based on scattering (or absorption) of a collimated light beam by the etched tracks have been developed.[103,104] Devices of this type makes it possible to determine a surface density of tracks in the range 10^4–10^7 cm^{-2}, but they require standards with known track density.

With the development of automation, it is becoming more and more common to obtain and analyze track images on a television screen. Using a light pencil, one can measure their parameters or convert the track images to analog form, using a computer for the analysis.[38] In auto-

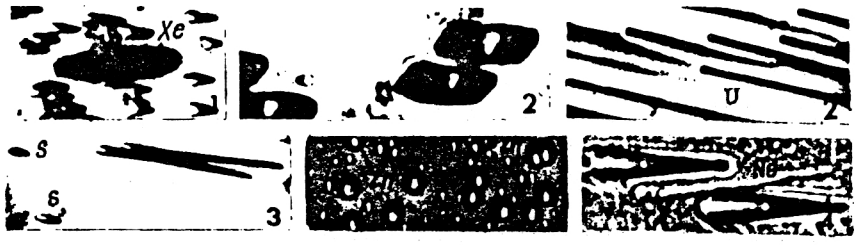

FIG. 8. Microphotographs of tracks of ions entering detectors at various angles: 1) PETP, Xe, and O ions (~1 MeV/amu), angle 30°; 2) mica, Xe (~ MeV/amu) and U (8.7 MeV/amu) ions, angle 30°; 3) phosphate and silicate glasses, Zn and S ions (~3 MeV/amu), angles 30 and 60°, respectively; 4) PAGC, Ne ions (3 MeV/amu), angle 30°.

matic scanning, two techniques are used to analyze the etched tracks. The first is "elimination" of "gray." In this technique, one considers only the parts of the image in which the density exceeds this established lower limit. The second technique is based on recognized properties of the shape. In this case, one attempts to eliminate an undesirable quality of the image, which cannot be done solely on the basis of the elimination of gray. Division according to shape is a difficult task for instrumental implementation, though for ions that enter the detectors at right angles the round track openings can be distinguished from other background defects, and they can be analyzed on the basis of the features of the openings. In other cases, analysis of the track shape requires long programs and long analysis times.

Detailed reviews and analysis of semiautomated and automated systems for the analysis for track information from SSNTDs can be found in Refs. 38 and 105–107.

2. DETECTION PROPERTIES OF SOLID-STATE NUCLEAR TRACK DETECTORS

The most important characteristics of SSNTDs are their sensitivity and charged-particle detection efficiency.

Sensitivity of SSNTDs

It follows from the track etching mechanism that the sensitivity of all SSNTDs has a threshold nature. As was shown earlier, the threshold is characterized by the minimum ionization density produced by the charged particle in the matter at which (and above) the track can be developed by etching, i.e., when $v_t \geqslant v_m$. The typical dependence of v_t/v_m on the ionization losses in PAGC is shown in Fig. 9. In the region of small ionization losses (region I), the dependence approaches unity asymptotically. This quantity characterizes the sensitivity threshold. In this region, the particle tracks have the form of low-contrast spots or etch-pits, whose parameters are not easily measured, and efficient detection cannot be achieved. From values $v_t/v_m \sim 2$, the track acquires a definite shape, and 100% detection efficiency can be achieved, especially in the counting regime. However, because of the weak dependence of v_t/v_m on the ionization in this region, identification or spectral measurements are difficult. Region II is characterized by maximum growth of the etching rate with increasing ionization loss and is of the greatest interest as regards both sensitivity and resolution. By resolution, we mean here discrimination of particles with low ionization powers. At still larger v_t/v_m, the linearity may cease to hold for some detectors (for example, cellulose nitrate) and etching regimes (insufficient exchange of reaction products in the case of very intense etching).[47,107]

In the microphotograph in Fig. 8 one can see tracks of ions for which $v_t/v_m \sim 2$ (sulfur), $v_t/v_m \sim 2$ (oxygen), and $v_t/v_m > 10$ (zinc and xenon).

To determine the sensitivity threshold the data are, as a rule, analyzed mathematically. For polymers, the dependence has the form

$$v_t/v_m = 1 + a(X)^b \quad \text{or} \quad v_t/v_m = a(X)^b,$$

where a and b are empirical coefficients. Instead of X one may have dI/dx, dE/dx, Z_{eff}/β, etc. Taking $v_t/v_m = 2$ as the beginning of the sensitive range, one can find the ionization at which tracks are developed with 100% detection efficiency. The coefficients a and b are found on the basis of calibration experiments. For various regimes and materials, their values are given in Refs. 47, 72, and 108–110.

One of the important characteristics of SSNTDs is correct reproduction of the range of the particle in the matter. For some inorganic insulating materials possessing a high sensitivity threshold, the final ionization before the stopping of the particle is insufficient to develop the damaged material. As a result, there is an ion range deficit ΔR.[8] For muscovite mica, Fig. 10 shows the experimentally obtained dependence of the range deficit ΔR on Z_{ion}, which must be taken into account in the analysis of physics experiments.[47] To determine the range deficit of heavy and light fragments in muscovite mica and phosphate glass, Gangrskiĭ *et al.*

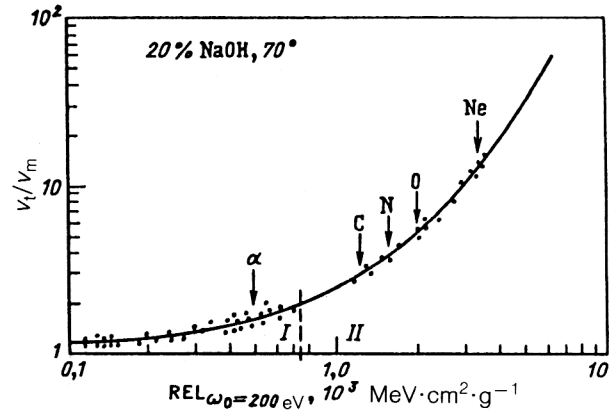

FIG. 9. Dependence of v_t/v_m on $REL_{\omega_0=200\ eV}$ for PAGC. The curve was obtained by fitting the experimental points. The vertical arrows indicate the regions of maximum ionization loss for the various ions; the numbers I and II correspond to different dependences of v_t (v_m) on REL (see the text).

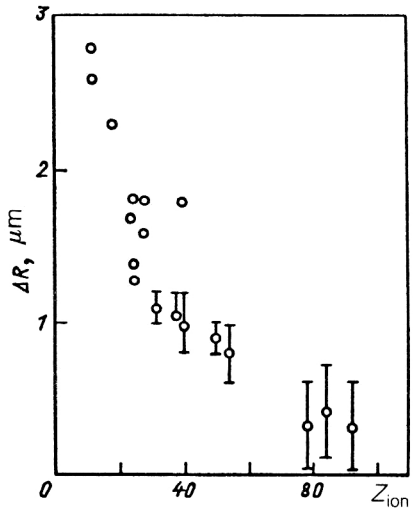

FIG. 10. Empirical dependence of the range deficit ΔR in muscovite mica on the ion charge Z_{ion}.

irradiated these detecting materials simultaneously with polycarbonate using Xe and Zr ions with energy ~1 MeV/amu. The polycarbonate registers the complete range of these ions. The range deficit of the fragments was determined from the comparative data and was 1.0–1.5 μm.

Detection efficiency

The detection efficiency is one of the most important criteria in the choice of a detector for physics investigations. The total detection efficiency can be defined as

$$\varepsilon_{tot}=\varepsilon\varepsilon_\delta .$$

The first term of the product depends on the detection threshold of the SSNTD and for particles entering at 90° is determined by comparison with the detection efficiency of another, more sensitive SSNTD. Thus, it was shown in Ref. 111 that the detection efficiency of phosphate glass and mica for Ne ions entering normally with energy near the ionization maximum is about 25% of the detection efficiency of PETP, in which all Ne ions of that energy are revealed by etching. Above the detection threshold, at $v_t/v_m \geqslant 2$, the value of ε is near unity. The geometrical factor ε_δ is determined by the critical angle of entry of the ion into the detector: $\delta_{cr}=\arcsin(v_t/v_m)$. In the case of homogeneous particles and a thin source, $\varepsilon_\delta=1-\sin\delta_{cr}$; for a thick source, $\varepsilon_\delta=\cos^2\delta$.[8]

Table III gives data on measurement of the critical angle and detection efficiency of fission fragments in some of the most frequently used materials,[47] and Table IV gives data for the widely used PAGC detector CR-39 (USA).

It can be seen that the materials in the table have high efficiencies of fission-fragment detection. In other cases, it is necessary to take into account v_t/v_m and to place the detector at a definite angle in order to obtain the maximum detection efficiency (sphere in 4π geometry, focal plane of spectrometer, separator, etc.).

To determine R_{eff} [the effective thickness of the layer of material for which all fission events of nuclei with known Z ($10 \leqslant Z \leqslant 92$) are detected in a given SSNTD], the empirical curve $R_{eff}(Z)$ was obtained in Ref. 112 together with a formula for calculating R_{eff} (mg/cm^2) in samples having complicated chemical compositions. For SSNTDs based on mica, PETP, and polycarbonate, the formula has the form $R_{eff}=0.046\Sigma_{i=1}^{n}a_iZ_i+0.78$, where a_i is the percentage content of element i in the detector, and Z_i is its atomic number.

The detection characteristics of the SSNTDs given in the tables can change under the influence of heating, moisture,[113] high exposure to radiation and ultraviolet light, and also during operation under vacuum conditions. The influence of temperature on the etchability of the latent tracks depends on the type of SSNTD and also on the stage at which the heating of it occurred: before, during, or after irradiation. This factor is important when the detectors are used in long physics experiments at high ion fluxes. It was shown in Refs. 114 and 115 that if the temperature is decreased during the time of irradiation, the etching rate of the material along the tracks of ions in polycarbonate, PAGC, and PETP increases. It was found that the thermal stability of the latent tracks depends on the type of SSNTD and on the specific energy loss. For inorganic detecting materials, it is higher. Table V gives the limiting temperature at which the latent tracks of fission fragments in some detecting materials can be preserved.

TABLE IV. Dependence of critical angle and detection efficiency of ions on REL in CR-39 (PAGC).

Ion species and energy, MeV		REL, MeV·cm^2·mg^{-1}	ε,%	δ_{cr}, deg
^{4}He	5,5	0,1	19,0	54
	3,0	0,3	50,0	30
	0,5	1,13	76,0	14
^{12}C	3,8	2,0	87,8	7,0
	2,5	3,0	93,0	4,0
^{20}Ne	5,7	4,0	96,5	2,0
	3,5	6,0	98,0	1,2

TABLE V. Temperatures at which fission-fragment tracks can be preserved, concentrations of impurity fissioning elements, and maximum radiation doses from some SSNTDs.

Detector type	Maximum temperature at which fission-fragment tracks are preserved, °C	Concentration of impurity fissioning elements, g/g	Maximum radiation dose D_{cr}, kGy
Muscovite mica (India)	650-700	10^{-7}-10^{-8}	$5\cdot10^{4}$
Glasses:			
silicate	300	10^{-3}-10^{-6}	$5\cdot10^{4}$
quartz	500	10^{-8}-10^{-13}	$5\cdot10^{4}$
phospha	300-500	10^{-7}-10^{-9}	
Polymers:			
polyethylene terephthalate	160	10^{-10}	$5\cdot10^{3}$
polycarbonate	160	10^{-10}	$5\cdot10^{2}$
cellulose nitrate	120	10^{-9}	10
poly-allyl-glycol-carbonate	180	10^{-9}	5

When polymers are heated, thermal-oxidation processes can take place, changing their properties. Annealing of PAGC before irradiation with α particles for 10–15 h at 100 °C increases v_t and v_m, although v_t/v_m is changed little.[47,115] If orientated polymers (polycarbonate, PETP) are heated, relaxation takes place, and the linear dimensions change. For example, PETP samples decreased in size by 15% after 1 h at 150 °C.[47] At $T\geqslant650$ °C, muscovite mica loses the crystallization water and ceases to detect particles. In contrast, phosphate glass does not change its detection properties even after melting (and cooling). It is assumed that the annealing of linear damaged regions takes place through diffusion of defects in the crystal lattice or the displacement of fragments of molecules in polymers. The authors of Refs. 35 and 43 proposed a two-zone model of tracks that satisfactorily explains the track regression in crystals by viscous laminar flow of interstitial atoms to the track axis, where there are excess vacancies. Annealing experiments for ions with various ionizing powers showed that the track sections corresponding to the highest ionization are most stable with respect to annealing.[47,116] Figure 11 shows the relative change in the track length of ions and fission fragments in muscovite mica as a function of the annealing temperature. The ion energy corresponds to the maximum of the Bragg ionization curve. By means of selective annealing of this type one can in fact change the sensitivity threshold of detection in mica. An increase of the detection threshold of crystalline detectors by annealing was also observed in other minerals and glasses (Refs. 5, 38, 117, and 118). It should be mentioned here that for each type of SSNTD there exists a definite degree of ionization at which ion tracks are not annealed.[5,47] For mica this is the case for iron ions, and for olivine it happens for particles with $Z\sim50$ and energy in the region of maximum ionization. In Refs. 5 and 8, this effect is attributed to saturation of the structure defects that appear in the crystals.

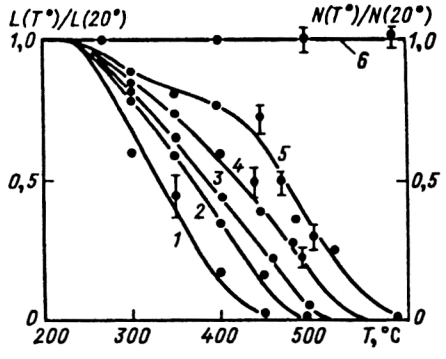

FIG. 11. Dependence of the relative change of the track length of the ions ^{40}Ar (1), ^{48}Ti (2), ^{54}Cr (3), and ^{56}Fm (4) and of ^{244}Cm fission fragments (5) on the temperature of heating. Curve 6 is the relative change in the number of fission fragments with change in the temperature of heating.

The influence of anisotropy of the structure of crystals persists after they have been annealed. After annealing of mica, it was found[35] that the tracks of fragments entering the detector at normal incidence are shortened significantly more than those of fragments entering at a small angle.

Effect of neutrons, γ rays, electrons, protons, and α particles

The effect of these particles on the radiation stability of SSNTDs and on their detection properties has been studied (Refs. 15, 38, and 119–121).

The neutron flux that develops during experiments on heavy ions does not have a direct effect on the SSNTD properties. Fast neutrons give rise to background recoil nuclei, which can be detected in high-sensitivity polymeric detectors.[122] The neutron sensitivity depends on the detection sensitivity of the detector and varies from $5\cdot10^{-5}$ (for PETP) to $5\cdot10^{-3}$ track/neutron (for PAGC).[47] It must be borne in mind that neutrons can induce fission of impurity uranium nuclei, the concentrations of which in some detecting materials are given in Table V.

Depending on the type of SSNTD and on the presence of oxygen, γ rays can give rise to various radiation effects. In some, an increase in the radiation dose is accompanied by an increase of the structuring, and the molecular mass can be changed; at low doses, cross-linking occurs, and at high doses there is destruction.[121–126] For example, for PETP the dose dependence can be divided into three regions (Fig. 12). In region A (D_γ=0–10^2 kGy), the material of the latent track changes its properties, and v_t in-

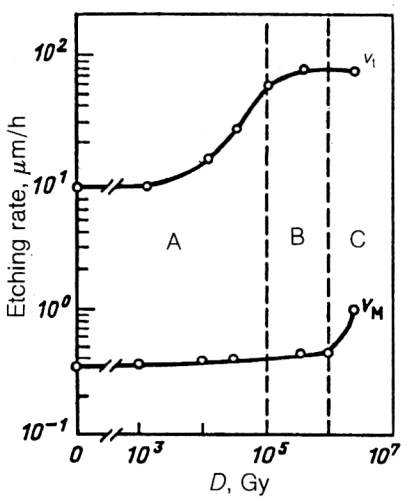

FIG. 12. Etching rates v_t and v_m of tracks of Ar ions entering PETP with energy 5.6 MeV/amu, as functions of the absorbed dose of γ radiation.

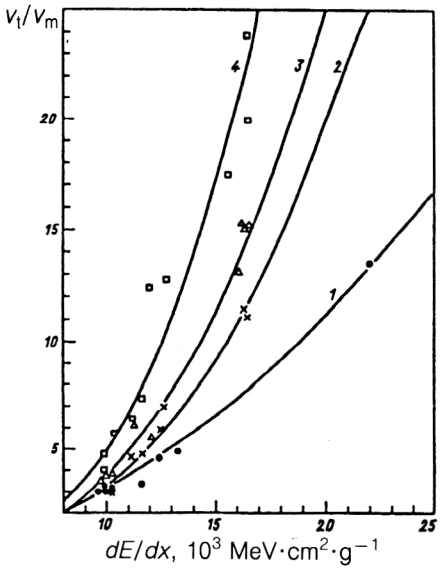

FIG. 13. Dependence of track etching selectivity v_t/v_m of various accelerated ions on dE/dx in PETP for additional irradiation with an α-particle flux of the following densities: 0–10^9 cm^{-2} (curve 1, black circles); $7\cdot10^9$ cm^{-2} (curve 2, crosses); $4\cdot10^{10}$ cm^{-2} (curve 3, open triangles); $1\cdot10^{12}$ cm^{-2} (curve 4, open squares). The curves were obtained by fitting the experimental points.

creases. In region B (up to $\sim10^3$ kGy), when the material of the latent track is completely changed, the properties of the surrounding material begin to change slowly, and v_m increases. In region C ($D_\gamma\sim10^4$ kGy), v_m increases strongly, and this leads to a decrease in v_t/v_m. It is best to work in region B. For other polymers, a different dose dependence can be observed.[126] In inorganic SSNTDs at doses $D\geqslant10^2$ MGy, fine tracks that make scanning difficult are formed.[126]

Electrons and protons in crystalline detectors induce defects at doses greater than 50 MGy.[128] Beginning at 220 MGy, they increase v_m and change the coloring of the detecting material, and also the track shape.[128]

In polymers, electrons, protons, and α particles can raise the etchability of latent tracks at certain fluxes, which are specific for the given detecting material. Thus, for PETP there was found to be a rising dependence of the change of v_t/v_m on the ionization losses of the ions with increasing α-particle flux, as shown in Fig. 13.[47] It can be seen that the chemical activity of the track material increases at flux densities greater than 10^9 cm^{-2}, especially in the region of large dE/dx. The value of v_m begins to increase only at $\sim10^{12}$ cm^{-2}.

It must be borne in mind that at high α-particle flux densities ($>10^{10}$ cm^{-2}) scattering processes give rise to a large number of recoil nuclei ($>10^6$ cm^{-2}), which, depending on the SSNTD sensitivity threshold, can give rise to etchable tracks and result in a deterioration of the conditions of scanning and measurment of the parameters of the etched tracks.

The presence of oxygen in a polymer during and after irradiation favors the formation of latent tracks. Irradiation in vacuum can significantly lower the etching selectivity.[129–131] If irradiated samples are kept in air and exposed to ultraviolet light (of an appropriate wavelength), the etchability of the latent tracks can be increased.[31,47,77] Figure 14 shows how the mean track length L and mean track diameter D of fission fragments (ff) and ^{20}Ne ions (2.3 MeV/amu) in PETP change with the time during which the material is kept in air after irradiation in vacuum.[47] Figure 15 shows the dependence of the time of exposure to ultraviolet light (in air) with $\lambda\geqslant320$ nm (at which v_t for the given ion reaches a maximum) on the specific energy loss dE/dx.[130] Photosensitizing is used to increase the etchability of ion tracks, especially if the irradiation occured in vacuum at a raised temperature.[130] Recently, it has been found possible to sensitize the region of a track by chemical solvents.[110]

It follows from analysis of the experimental data that the sensitivity thresholds of SSNTDs can be changed in a desired direction by chemical processing, heating, and also by means of ultraviolet, γ, and α radiation.

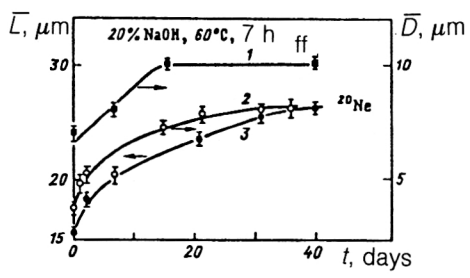

FIG. 14. Mean diameters (1, 2) and length (3) of ^{244}Cm fission-fragment tracks (ff) and ^{20}Ne tracks (2.3 MeV/amu) in PETP as functions of the time during which the SSNTD is kept in air after irradiation in a vacuum (10^{-7}–10^{-4} Pa).

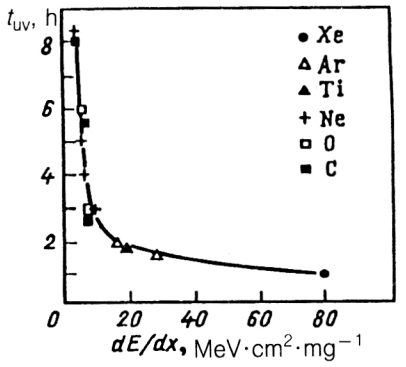

FIG. 15. Time of exposure to ultraviolet light for which v_t of the ion track reaches a maximum, as a function of dE/dx of various ions.

3. IDENTIFICATION OF CHARGED PARTICLES

To identify particles detected in SSNTDs, it is necessary to establish a connection between the parameters of the track and of the particle, i.e., the mass, charge, and energy. These particle parameters can be determined by measuring the rate of etching of the material along the track, v_t (a quantity proportional to the energy loss), and the particle range R in the SSNTD (a quantity proportional to the energy of the particle). However, the ionization curves of the dependence on the ion energies are rather complicated, and, as a result, it is not possible to propose a single principle of particle identification based on the parameters of the observed track and valid for the complete range of energies. Therefore, the problem of the identification of charged particles in SSNTDs depends on the energy range of the detected particles. Several methods of identification based on the ionization losses and ranges of the measured particles in chosen detectors have been tested and successfully used in various experiments.

Threshold discrimination of ions

As can be seen from Table I and Fig. 2, one can, on the basis of the conditions of the experiment and the sensitivity of the detecting materials, choose a type of material or a set of different materials (pile) to achieve the most effective identification of all particles. In addition, as was shown earlier, it is possible to change the detection threshold in a desired direction. For example a dose $\sim 2\cdot 10^5$ Gy of γ rays lowers the sensitivity threshold of PETP and makes it possible to detect carbon ions with $E\sim 20$ MeV as opposed to 12 MeV. Selective annealing raises the sensitivity threshold of crystals (mica, olivine, etc.) and makes it easier to identify highly ionizing particles.[47,132]

Above-threshold identification of particles

In above-threshold identification, one is dealing with the region of ion energy loss exceeding the threshold values for the given detecting material. For the identification of highly ionizing particles, one usually uses the $R(E)$ method, in which the energy of ions of one species is determined from the length of completely etched tracks and comparison of it with calibration or calculated range–energy data for the given material of the SSNTD.[15–18]

To obtain the energy and mass distributions of correlated pairs of fission fragments, one can use the relation[133]

$$R = CA^{-1/6}E^{1/2}, \tag{9}$$

where C is an empirical coefficient, A is the fragment mass, and E is its energy.[134,135] For example, Fig. 16 shows a two-dimensional distribution of the ranges of correlated fragments of neutron-induced ^{235}U fission.[130]

Each point of this two-dimensional graph corresponds to a pair of fission fragments having ranges R_1 and R_2, while the lines correspond to a constant mass ratio of the fragments. Each pair of fragments, with ranges $R_1 \pm \Delta R_1$

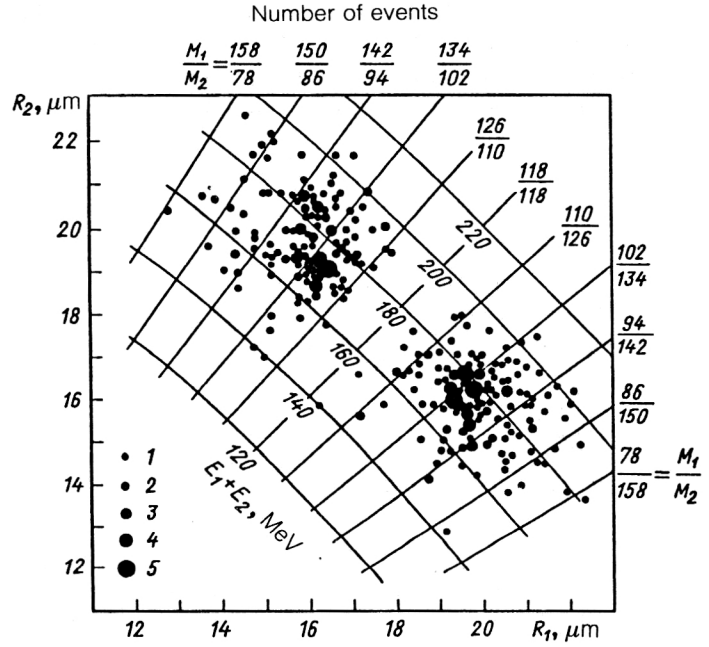

FIG. 16. Range distributions of correlated fragments (R_1 and R_2) from induced fission of ^{235}U.

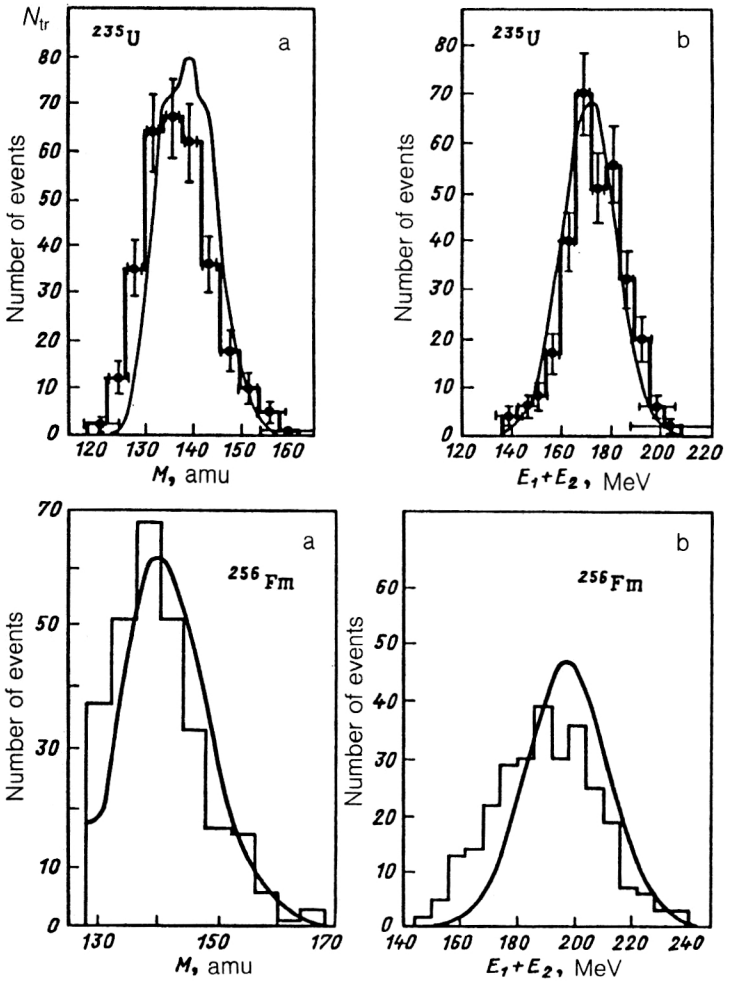

FIG. 17. Histograms of mass (a) and energy (b) distributions of fragments (E_1+E_2) of induced fission of ^{235}U and spontaneous fission of ^{256}Fm obtained in Ref. 133 by means of an SSNTD (polycarbonate) and analogous results obtained by means of semiconductor detectors (curves).

and $R_2 \pm \Delta R_2$, gives fragment masses $M_1 \pm \Delta M_1$ and $M_2 \pm \Delta M_2$. The relation (9) is used to obtain the distribution of the kinetic energies of the fission fragments. Figure 17 gives the mass and energy (total kinetic energy: TKE) distributions of fragments of the fission of ^{235}U by thermal neutrons and spontaneous fission of ^{256}Fm obtained in the ^{249}Bk$+^{22}$Ne reaction. The error in the determination of the atomic number does not exceed ± 2, and that of the energy, ± 3 MeV; only in the "tail" of the distribution does it increase. This method was used in experiments to study the spontaneous fission of short-lived nuclei.[130,136]

To identify particles with short range (energy $\leqslant 1$ MeV/amu), the dependence $D(E)$ is used. In this case, one etches the detecting material in such a way that the radius of the entry opening of the etched track of an ion entering the detector at a right angle is equal to the track range or greater than it. In this case, the area S of the entry opening of the ion track is proportional to the velocity v of the fission fragment of mass M and charge Z:[66]

$$S \sim v_m t M Z^{-2/3} v,$$

where t is the time of etching of the detector at the rate v_m. Since $v=(2E/M)^{1/2}$, it follows that $S \sim E^{1/2}$ and $D \sim E^{1/4}$. This relation was verified experimentally in Refs. 47, 65, and 66. The dependence $D(E)$ for various ions detected in phosphate glasses of different compositions is shown in Fig. 18. Up to $E \sim 60$ MeV, a proportional dependence of D on E is observed, but beginning with $E \gg 60$ MeV and $D > 80$ the dependence $D(E)$ is weaker and the resolution is poorer. At these energies, the ion range increases, and the $R(E)$ method can be used. By means of this method, one can study the energy spectra of the fragments of spontaneous fission. The energy distribution of ^{252}Cf fission fragments in phosphate glass[66] (with resolution down to ~ 2 MeV) is well correlated with data obtained by semiconductor detectors.

To study fission or nuclear fragmentation processes in which the reaction products have a wide spectrum of masses, charges, and energies, and are also emitted at very varied angles relative to the beam of projectile particles, it was proposed in Ref. 137 to use the method of successive etching,[138] which, depending on the etching time, permits a preliminary differentiation of particles according to their energies and masses. At each stage of the etching, the values of v are obtained through the track parameters. Then, using calibration dependences $v(dE/dx)$ and formulas for calculating the track etching figures from Ref. 86, one can calculate for all ions the dependences $v=f(E)$ and $D(d)=f(E)$ (D and d are the major and minor diameters of the entrance opening of the track of a particle that enters the SSNTD at an angle to the surface). Comparing the param-

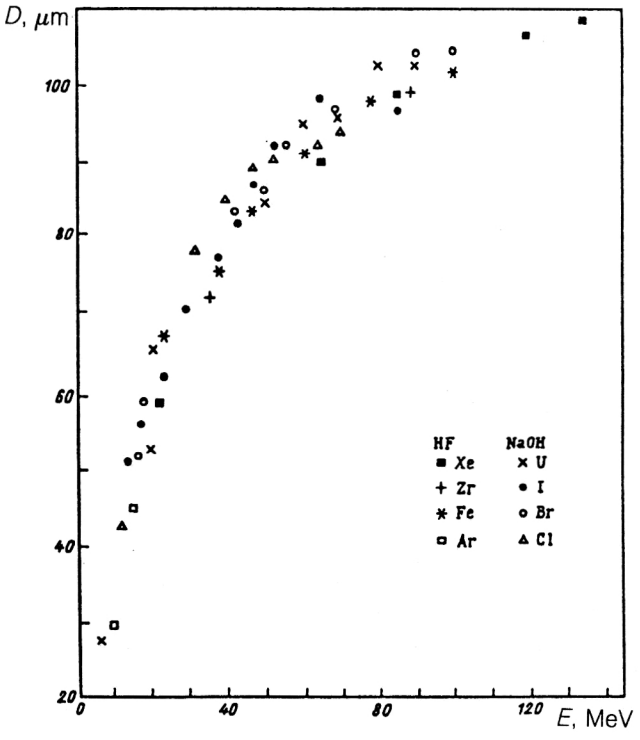

FIG. 18. Energy dependence of the track diameters of ions entering, at normal incidence, the surface of phosphate glasses of various compositions with the use of different solutions for etching: HF (Ref. 47) and NaOH (Ref. 66).

eters of each of the measured tracks with the calibration dependences $v=f(E)$ and $D(d)=f(E)$, it is possible to establish the nature of the charged particles. Charge resolutions $\Delta Z=\pm 0.5$ were obtained. The method was successfully used[137,139] to investigate ^{24}Mg and ^{28}Si decay.

To identify weakly ionizing particles, the $L(R_{res})$ and $v(R_{res})$ methods are used, assuming that there is a one-to-one relationship between the rate v_t at a given point of the track and the energy loss. Determination of the charge and mass is based on the relationship between the energy loss and the residual range. As was shown earlier, the dependences that describe the track etching process contain unknown constants, which are obtained by a choice of parameters. To find a semiempirical dependence of v_t/v_m on the charge and velocity of the particles, experimentally obtained dependences $v_t(R_{res})$ for ions with known masses, charges, and energies are used.

Several methods have been developed for making such measurements. The four that are most often used are represented schematically in Fig. 19. The first shows the ratio of the etched length L and the residual range R_{res} of an ion that has passed through two films of a pile and stopped in the third. Etching under the same conditions gives a set of lengths L of the etch-pits and the corresponding residual ranges R_{res}. From the range–energy relations for each range one can obtain the energy and, therefore, the ionization. The presence of several films makes it possible to measure several L_i and R_{ires}, and this increases the accuracy of the method (Refs. 8, 38, 47, and 72). In another

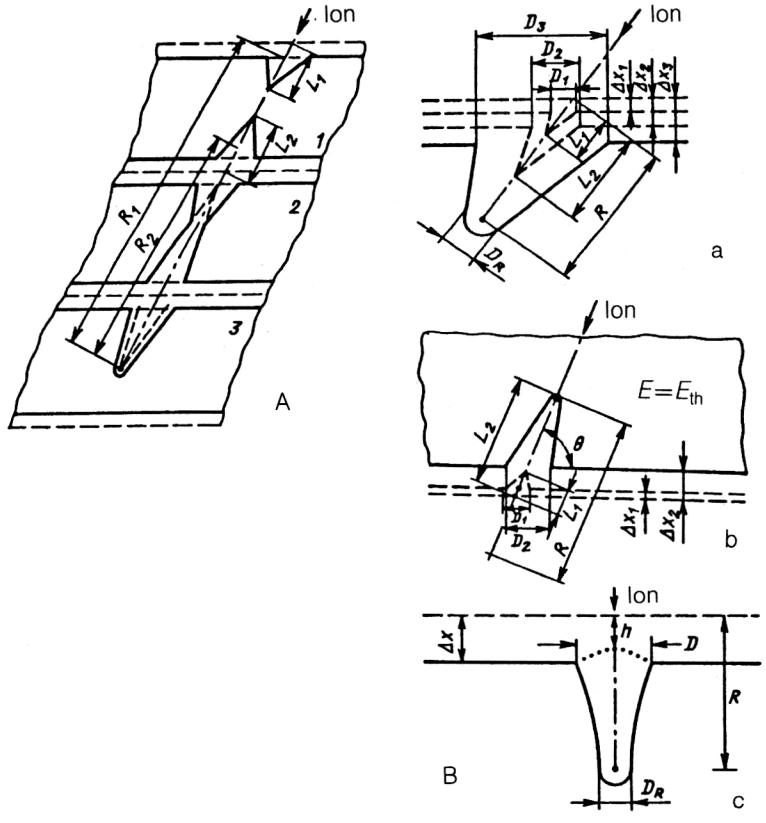

FIG. 19. Schematic representation of some methods of ion identification by measurement of the etched cone L or the etching selectivity v_t/v_m and the corresponding residual range R_{res} in several films of detecting material (A) and in one film (B) in the case of multiple etching of the film from the side of entry of the ion into the film (a) and from the opposite side (b), and also for a single etching of the tracks of ions with direction perpendicular to the detector surface (track-profile method) (c). In Fig. 19B, (a) and (b) show the results of triple and double etching of the detector material. In all the figures, the arrow indicates the direction of motion of the ion, and the chain line shows the ion trajectory; Δx is the thickness of the etched layer, and the broken lines show the initial surface of the film of detecting material.

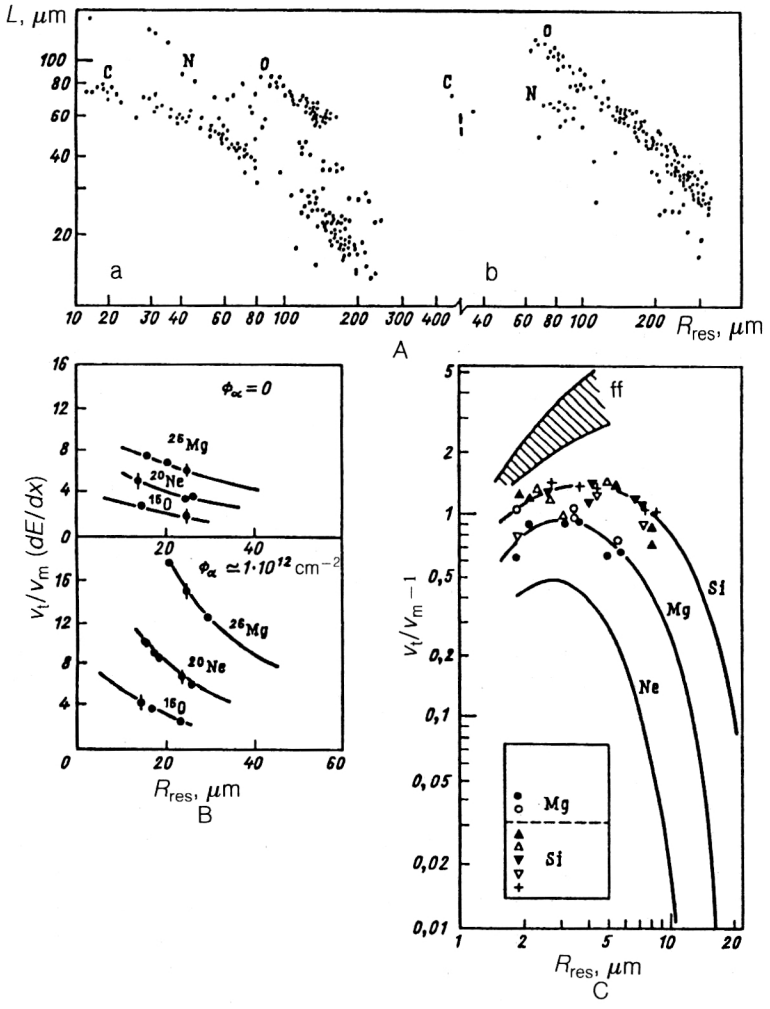

FIG. 20. Identification of ions by various SSNTDs: (A) the C, N, O group in accordance with the scheme of Fig. 19A, detected in cosmic rays in cellulose nitrate during a solar flare (a) and during the quiescent sun (b);[47] (B) corresponds to identification of ^{16}O, ^{20}Ne, and ^{26}Mg in accordance with the scheme of Fig. 19a, detected in PETP without additional treatment and for an α-ray flux density of order 10^{12} cm^{-2} (the points are the experimental data, and the curves are calculated); (C) C, O, Ne, Mg and fragments of spontaneous fission (ff) in accordance with the scheme of Fig. 19c, detected in phosphate glass from ^{238}Pu decay.[142]

case (Fig. 19B), the particle is detected in one film. To obtain several values of L and R_{res} (and, accordingly, v_t), it is necessary to etch the detecting material and measure the track length several times. A detailed analysis of results is presented in Refs. 73 and 140. To determine the Z of the track-forming particle, the experimental data are compared with calibration curves $L(R_{res})$. This identification method is actually a modification of the well-known (dE/dE)–E method, since the pit parameters characterize the ionization, and the residual range R_{res} characterizes the energy.

Using a two-stage etching of the track and a special treatment of polycarbonate, the authors of Ref. 141 obtained a definite track shape, and from its parameters they could obtain the dependences v_t(REL) and $v_t(R_{res})$. The method was used to identify low-energy ions with $8 \leqslant Z \leqslant 20$.

Besides measurement of track pits, the track-profile method[8] is used to obtain the dependence $v_t(R_{res})$. In this method, one measures the parameters of replicas of the tracks of ions that enter the detector at angle 90° (Fig. 19c). Figure 20 shows some results of the identification of nuclei by the methods just considered.[47,142]

For tracks with low etching selectivity ($v_t/v_m < 3$), when the length of the etched cone is very small,[108] the $D(dE/dx)$ method is used. In this case, the track diameter D is a more sensitive function of the ionization than its length. As a rule, normal incidence of the particles on the detector is used. If the particle has a range greater than the thickness of the detecting material (or a pile of detecting layers), then identification is aided by measurement of the entry and exit track diameters using two-sided etching of each film of detecting material. If the range is less than the thickness of the film (or of the pile of films), then the end of the track can be revealed by etching, and the particle range can be determined. Measuring the track diameter, one can determine the ionization loss of the ion from the dependence of D on REL (Fig. 21). With allowance for the function $R(E)$, it is possible to obtain the dependence $D(R_{res})$ and to identify the particles.[143,144] By using several films (a pile), it is possible to identify ions with higher resolution (Fig. 22).[143] A description of other identification methods can be found in Refs. 8, 38, and 72.

Errors of measurements

In all the identification methods (except the threshold method), data on the main track parameters—the length and diameter—are obtained by means of an optical microscope. The absolute error in the measurements for an individual track is ± 0.3 μm. The relative error in such measurements depends strongly on the size of the fully etched

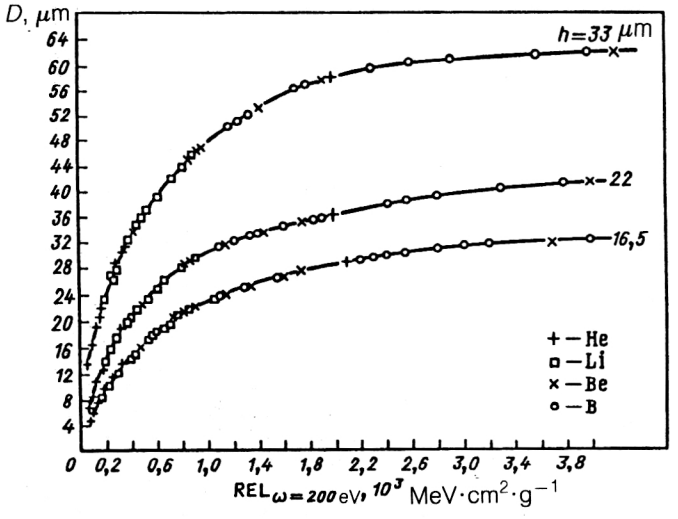

FIG. 21. Dependence of the particle track diameter on REL for $h=16.5$, 22.0, and 33.0 μm.

tracks. Experiments showed that in polymers, beginning with track diameters greater than 50 μm, the developed structure limits the accuracy of measurement. In glasses, the situation is better, and tracks can be etched to diameter 80–100 μm. For determination of the energy from the track length, the relative error in the measurement is between 5 and 0.2%, and for determination of the ionization from the track length it is ~0.6% for polymers and ~0.3% for phosphate glass. For very short tracks and small diameters, the errors may reach 10–20%. These errors are given for materials with isotropic properties. As regards crystalline materials with anisotropic structures and properties, it is difficult to use them for spectrometric measurements.

Width of the energy distribution

Figure 23 shows spectra of track lengths of ions measured in PAGC in various energy ranges. From comparison of these figures it can be seen that for particles with etched track length $\geqslant 80$ μm the measured spread is ± 1.4%. The energy of short-range particles with ionizing power close to that of fission fragments can be measured with an error ±3%. The accuracy of the energy measurement can be strongly affected by charge straggling of ions, which arises when they are stopped in insulating detecting material. It is not possible to separate this process from the total measured spread. Some comparative data on estimates of the straggling in SSNTDs are given in Table VI.[47]

The estimates show that for $E \leqslant 0.1$ MeV/amu the straggling leads to an energy spread of about 7%. The measured dispersion $W(\Delta E)_{0.5}/E$ of the spectrum is 10–20%. This indicates that the straggling makes an important contribution to the measured energy spectrum of the particles in the complete considered energy range.

The spectral distribution of tracks of α particles from ^{226}Ra in PAGC with respect to the track diameter (Fig. 24) shows that the resolution in this range of energies is not less than ±3%. This also corresponds to the energy resolution. In Ref. 145 measurements were made of the ranges of α particles in PAGC, and the energy resolution was determined for the interval 3–6 MeV and typical conditions of chemical treatment. It was shown that for 3-

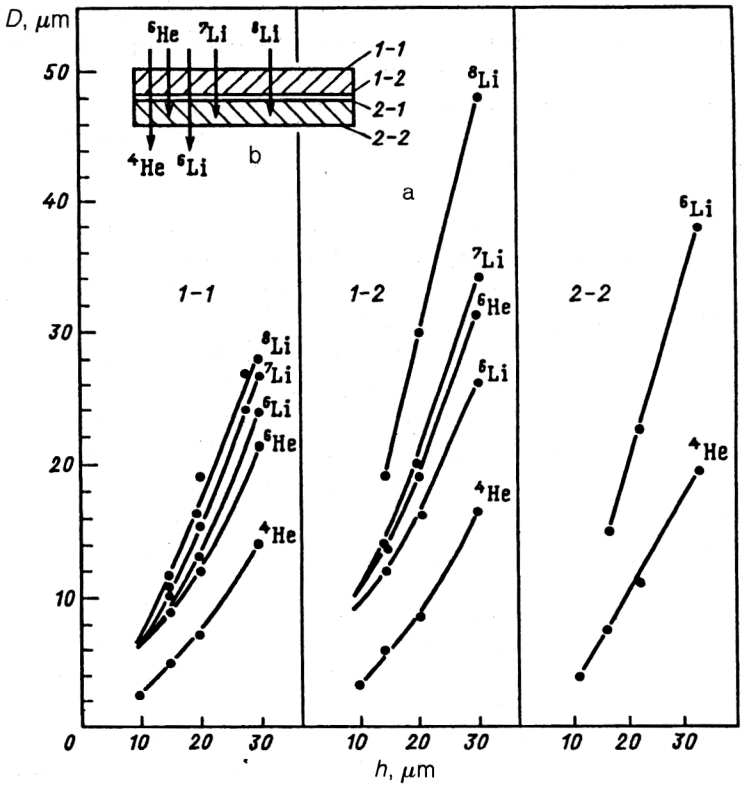

FIG. 22. Identification of helium and lithium isotopes in a two-film PAGC detector as a function of the etched film of detecting material in 20% NaOH at 70 °C.

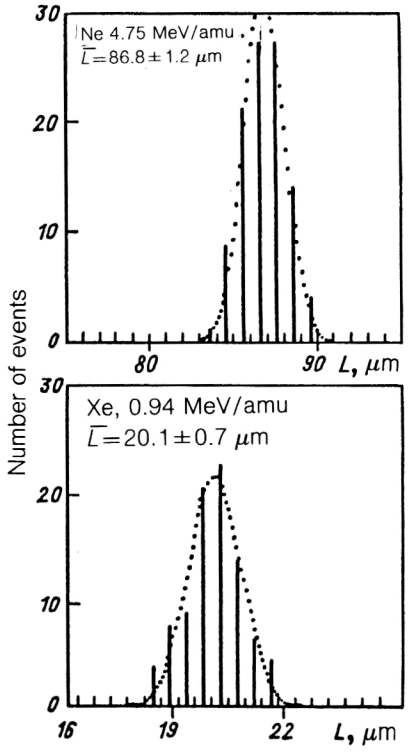

FIG. 23. Spectral distribution of track lengths of ions of Ne (4.75 MeV/amu) and Xe (0.94 MeV/amu) in PAGC.

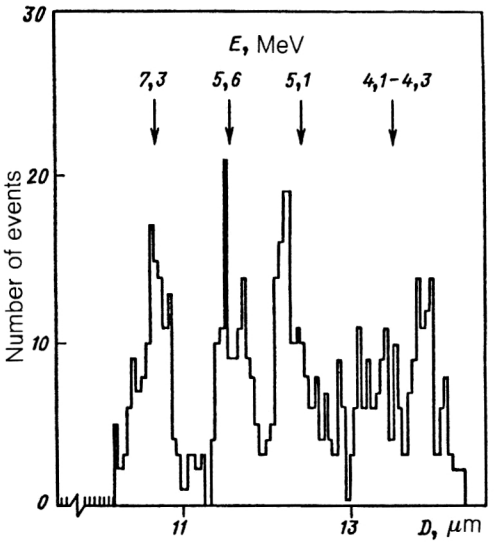

FIG. 24. Spectral distributions of track diameters of α particles from ^{226}Ra in PAGC.

MeV α particles the achieved energy resolution of 40 keV is limited by straggling; for 6 MeV, it is 35 keV for individual particles and 20 keV for a group of particles. The authors of the study succeeded in distinguishing groups of ^{252}Cf α particles with energies 6.076 and 6.119 MeV.

Accuracy of charge measurements

The etching selectivity v is directly related to the ionization loss, which is more sensitive to the charge of a particle than to the energy.

Figure 20A shows the results of identification of C, N, and O nuclei in cosmic rays.[47] One can see how particles with neighboring charges are identified. Analysis of the results by the χ^2 method shows that the charge resolution for light ions may reach ± 0.2.

In Ref. 143, He and Li isotopes, which have different rates of ionization loss (REL) were identified in PAGC. Good separation of the isotopes with respect to the charge and mass numbers was obtained (Fig. 25). There are several possibilities for some SSNTDs to increase their sensitivity by exposing the region of a latent track to additional radiation (ultraviolet, γ rays, etc.). Figure 20B shows measurements of $v_t/v_m(R_{res})$ for ^{26}Mg, ^{20}Ne, and ^{16}O ions in PETP before and after irradiation of the detectors with an α-particle flux with a density of order 10^{12} cm^{-2} (Ref. 47). It can be seen that the etching selectivity and charge resolution were increased by a factor of about 2. The use of additional radiation makes it possible in particle identification to improve the resolution of ions with nearly equal Z even in the most unfavorable region of detection with respect to the energy. Thus, summarizing the detection possibilities of SSNTDs, we must say that they are capable of detecting and identifying with high efficiency a wide range of heavy ions, discriminating both energies and charges.

4. USE OF SOLID-STATE NUCLEAR TRACK DETECTORS IN NUCLEAR-PHYSICS EXPERIMENTS

The high charge resolution of SSNTDs, their low sensitivity to light charged particles, the discrimination of par-

TABLE VI. Comparative data on estimates of straggling from experimentally determined scatter of track lengths.

Ion	E, MeV/amu	ΔE, MeV	$\Delta E_{str}/E$,%	$W(\Delta E)_{0,5}/E$,%
	1,0	0,335	1,5	3,0
^{22}Ne	2,5	0,530	1,0	2,0
	4,75	0,730	0,7	1,4
	0,94	2,1	1,7	3,6
^{132}Xe	2,5	3,5	1,0	2,5
	10,6	7,2	0,5	0,9

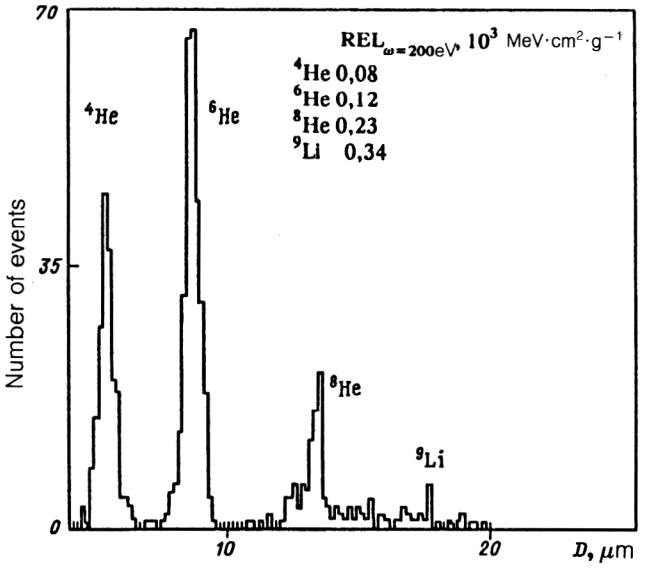

FIG. 25. Spectral distribution of track diameters of He and Li isotopes having different $REL_{\omega=200\,eV}$.

ticles with respect to charge by the choice of the detector material, and the possibility of using large areas made it possible to carry out important experiments in various directions of heavy-ion nuclear physics in cases in which a high energy resolution is not required (for SSNTDs, $E/\Delta E \sim 10$–50). Here we shall review some fields of nuclear-physics investigations in which SSNTDs are fairly widely used.

Study of radioactive decay of natural elements. Alpha decay

According to the sensitivity threshold of SSNTDs (see Table I), α particles can create etchable tracks in some of them, but the range of α-particle energies in which this occurs is bounded by two energies E_{min} and E_{max}, at which v_t is close to v_m and it is difficult to recognize the tracks. Table VII gives energy limits for α-particle detection in some plastics.

By using SSNTDs, one can determine with high accuracy (of order 1 μm) the spatial distribution of an α-active isotope in radioactive targets and monitor possible contamination of physics facilities. It must be borne in mind that if α-sensitive detectors are kept in air, they can accumulate tracks of α particles from the decay of radon and its radioactive decay products contained in the ambient atmosphere.

Cluster radioactivity of heavy nuclei

The discovery of a new type of radioactivity with emission of ^{14}C nuclei[146,147] confirmed theoretical predictions of the existence of a form of nuclear decay[148] intermediate between α decay and spontaneous fission. These experiments showed that the probability of ^{14}C emission is almost 10 orders of magnitude less than the probability of α decay. It was seen from the calculations that the emission of heavier clusters from nuclei with $Z > 90$ must occur with much lower probability.[148] Electronic detection methods were used to look for ^{14}C clusters. However, they have significant limitations with respect to the number of incident α particles and the target thickness, and the detection efficiency is low ($< 1\%$). Ions with $Z \geqslant 6$ and energy 30–85 MeV are most effectively detected by SSNTDs. The threshold sensitivity of the detectors, the possibility of using large areas (up to 10^3 cm^2) and, therefore, the large amounts of investigated matter, and the high detection efficiency have made it possible to raise the sensitivity of the method by several orders of magnitude compared with the electronic method. Work was done mainly by two groups of investigators—in laboratories at Berkeley and Dubna.[142,149] Polycarbonate, PETP, and phosphate glass were used in the SSNTDs. The American scientists used the replica method to find and analyze cluster tracks, while the Dubna scientists used multiple etching (see Fig. 19B). The identification was by the $v_t/v_m(R_{res})$ method. The energy was determined by measuring the total range of the clusters, and a mass number was found from the reaction Q value.[147] The method made it possible to achieve resolutions $\Delta Z = \pm 0.2$ for the charge, $\Delta M = \pm 1$ for the mass, and 3–5% for the energy (Figs. 26 and 27).

High α-particle flux densities ($> 10^{11}$ cm^{-2}) gave rise to background etchable tracks of recoil nuclei produced by the decay of α particles on nuclei of the detecting material. They hindered the search for events and distorted the shape of the tracks being sought. Therefore, if spectrometric measurements are being made, there exists a limit on the α-particle flux density for polycarbonate, PETP, and phosphate glass detectors of order 10^{10}, 10^{12}, and 10^{14} cm^{-2}, respectively. For reliable detection of clusters under conditions of a high background of α particles and fission fragments with flux densities up to 10^{15} and 10^6 cm^{-2}, respectively, a two-layer detector was developed at Dubna, its thin upper layer (6–10 μm) being removed after etching together with the tracks of the recoil nuclei.

In Table VIII, we give the results of investigations of cluster decay of heavy nuclei by SSNTDs.

The use of SSNTDs led to cluster emission from 12

TABLE VII. Limits of energies for α-particle detection in some polymeric nuclear track detectors.

Detector type	E_{min}, MeV	E_{max}, MeV
Polycarbonate	0,2	3
Cellulose nitrate	0,1	4–6
Poly-allyl-glycol-carbonate	0,1	85

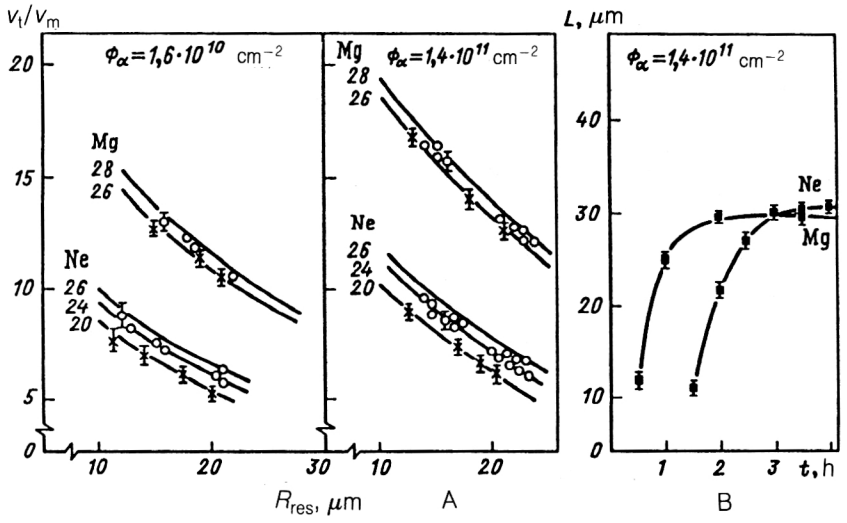

FIG. 26. Cluster identification: (A) dependence of v_t/v_m on R_{res} (PETP); the curves are calculated, the crosses show the results of calibration experiments, and the open circles are the experimental results on cluster decay of ^{234}U nuclei; (B) dependence of the etched length L of the tracks of neon and magnesium ions emitted as a result of ^{234}U decay as a function of the etching time t.

isotopes; moreover, the emission of two types of cluster was observed from ^{234}U and ^{238}Pu nuclei, the two types being identified by the rate of etching of their tracks (Fig. 26A). A more detailed review of this problem is given in Refs. 142 and 149.

Spontaneously fissioning nuclei. Searches for superheavy elements in nature

Solid-state nuclear track detectors are widely used to determine the activity and distribution of spontaneously fissioning nuclei in samples and targets (Refs. 5, 8, 38, and 47), and also to determine and verify more accurately the half-lives of spontaneously fissioning isotopes, for example, ^{238}U (Ref. 150) and ^{240}Cf (Ref. 151). This is done by means of detecting materials with a low concentration of impurity uranium nuclei (polymers, quartz, and phosphate glasses) (see Table V).

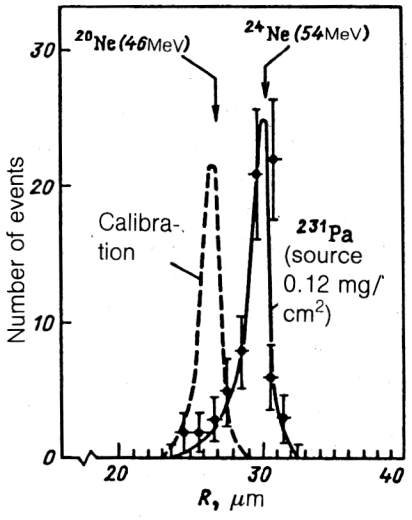

FIG. 27. Distribution of ranges R of clusters in PETP emitted as a result of ^{231}Pa decay with indication (by the arrow) of the range of an expected ^{24}Ne cluster with $E=54$ MeV and calibration ^{20}Ne ions with $E=46$ MeV.

In addition, SSNTDs can be used to study the energy and mass distribution of the fission fragments of spontaneously fissioning nuclei by measuring the diameters or lengths of the fragment tracks. For example, in Refs. 65 and 66 a specially developed phosphate glass (with detection threshold around 9 MeV) was used to obtain an energy resolution of 1–2 MeV for track diameters 150–200 μm of fragments (entering the SSNTD at right angles). As an example, Fig. 28 shows the energy distribution of ^{252}Cf fission fragments obtained by means of the phosphate glass in a comparison with measurements made by a semiconductor detector.[66] Similar results were obtained with a phosphate glass of different composition in the study of Ref. 65. Placing a thin absorber between the SSNTD and the source, the authors of Refs. 152 and 153 succeeded in determining the energies of the light and heavy fragments of Th, U, and Pu fission with an error of about 3% by measuring the track diameters in silicate glass.

In the case of irradiation in 2π geometry, methods based on measurement of v_t/v_m and of the total length of etched fission-fragment tracks are used.[133–136] In Refs. 134 and 135, polycarbonate and cellulose triacetate SSNTDs were used in the first approach to determine the atomic number with accuracy ± 1.5 for the light fragment and ± 2.0 for the heavy fragment. The energy spread was $\pm$ 5%. The second method has been treated in Sec. 3 of this review.

The publication of papers predicting the possible existence of superheavy nuclei in the region $Z=114$ and $N=184$ of doubly closed shells, and relatively stable with respect to α decay and spontaneous fission, created great interest and stimulated many experiments to look for superheavy elements in both terrestrial and extraterrestrial (meteorite and lunar) samples.[154–166]

Since it is difficult to separate α particles belonging to the sought-for element from background α particles, spontaneous fission was mainly investigated. It was assumed that after α decay superheavy elements in the region of ~ 114 isotopes must fission spontaneously. The accuracy of the calculation of the half-lives of superheavy elements is low—the theory allows the existence of nuclei with half-

TABLE VIII. Relative probability of emission of $Z > 10$ clusters.[142]

Initial nucleus and emitted cluster	Kinetic energy of cluster, MeV	Measurements $\log T^{*}_{1/2}$	$-\log(\lambda_{cl}/\lambda_{\alpha})^{**}$
$^{221}Fr(^{14}C)$	29,28	>15,77	>13,3
$^{221}Ra(^{14}C)$	30,34	>14,35	>12,9
$^{222}Ra(^{14}C)$	30,97	11,02±0,06	9,43±0,06
$^{223}Ra(^{14}C)$	29,85	15,2±0,05	9,21±0,05
$^{224}Ra(^{14}C)$	28,63	15,9±0,12	10,37±0,12
$^{225}Ac(^{14}C)$	28,57	>18,34	>12,4
$^{226}Ra(^{14}C)$	26,46	21,33±0,20	10,6±0,20
$^{231}Pa(^{23}F)$	46,68	>24,61	>12,74
$^{230}Th(^{24}Ne)$	51,75	24,64±0,07	12,25±0,07
$^{232}Th(^{26}Ne)$	49,70	>27,94	>10,3
$^{231}Pa(^{24}Ne)$	54,14	23,23±0,08	11,22±0,08
$^{232}U(^{24}Ne)$	55,86	21,06±0,10	11,7±0,10
$^{233}U(^{24}Ne)$	54,27	24,82±0,15	12,12±0,15
$^{233}U(^{25}Ne)$	54,32	24,82±0,15	12,12±0,15
$^{234}U(^{24}Ne)$	52,81		
$^{234}U(^{26}Ne)$	52,87	25,25±0,05	12,36±0,05
$^{234}U(^{28}Mg)$	65,26	25,75±0,06	12,86±0,06
$^{237}Np(^{30}Mg)$	65,52	>27,27	>13,4
$^{238}Pu(^{30}Mg)$	67,00		
$^{238}Pu(^{28}Mg)$	62,00	25,7±0,25	16,25±0,25
$^{236}Pu(^{28}Mg)$	61,6	21,7	~14,3
$^{238}Pu(^{32}Si)$	78,95	25,3±0,16	15,86±0,16
$^{241}Am(^{34}Si)$	80,60	>25,3	>15,1; 14,1

*$T_{1/2}$ (sec) is the partial half-life of the nucleus.

**λ_{cl} and λ_{α} are the cluster and α-decay constants of the nucleus.

lives longer than for uranium nuclei but with the same probability predicts half lives less than fractions of a second, and this casts doubt on the conjecture that such nuclei exist.

Searches for superheavy elements in various samples by means of SSNTDs were made in two main directions. First, investigations were made of crystals and glasses that themselves register tracks and could have accumulated information over the long period of their existence. In the second approach, investigated samples were placed between SSNTDs for a long exposure duration. In both cases, the investigators looked for an excess density of fission-fragment tracks compared with the density of tracks from the spontaneous fission of nuclei of natural actinides (^{238}U and ^{244}Pu in minerals from meteorites). Under the assumption that 100% of the nuclei of the sought-for superheavy element (or daughter elements resulting from series of α decays) undergo spontaneous fission,[155] a lower limit on the concentration of superheavy elements in samples containing 10^{-6}–10^{-7} g/g of uranium can be obtained at the level 10^{-12}–10^{-13} g/g.

To improve the identification and sensitivity of the search for fragment tracks in crystals, selective annealing of tracks was used in the studies of Refs. 156–159. It was shown that for a certain annealing regime the tracks of light fragments of actinides become shorter more rapidly than the tracks of heavy fragments. After such treatment, the spectra of fragment track lengths in the investigated minerals must contain two groups corresponding to spontaneous fission of the actinides and the superheavy elements. Investigation of apatites by this method showed that the concentration of superheavy elements (with $T_{1/2} \sim 10^{9}$ yr) is not more than 10^{-13} g/g.

Another search method was associated with the conjecture of triple fission of nuclei of superheavy elements and the possibility of identification of it by three-prong tracks.[160] The investigators assumed an increase in the sensitivity of the method by about 100 times. However, the experiments made with apatite and mica samples established only upper limits for the concentration of superheavy elements: in apatite $\sim 10^{-13}$ g/g for uranium con-

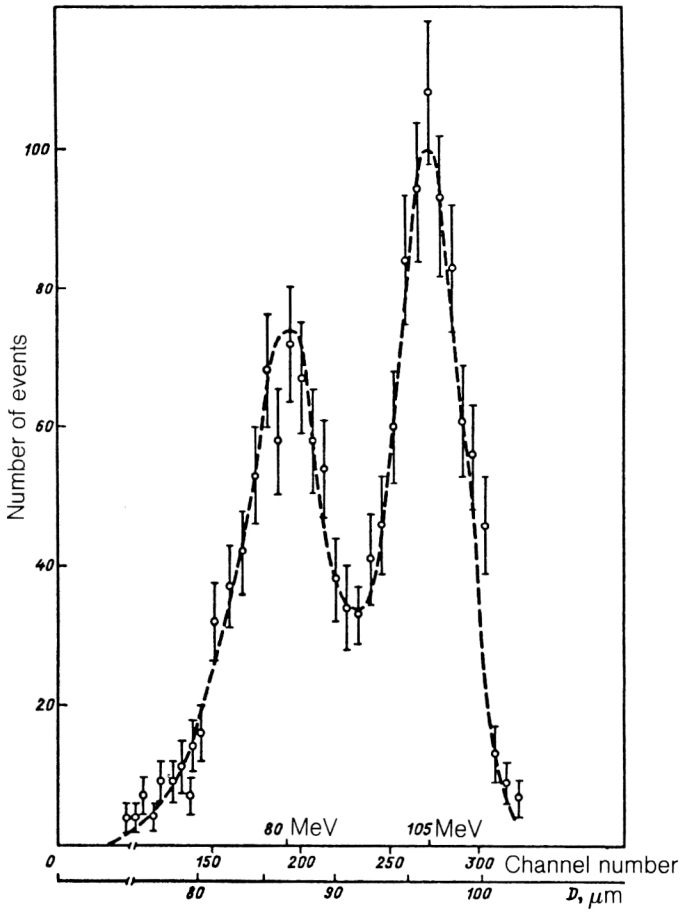

FIG. 28. Energy distribution of ^{252}Cf fission fragments obtained by a SSNTD (points) and by a semiconductor detector (broken curve).

centration $\sim 2 \cdot 10^{-6}$ g/g, and for mica $5 \cdot 10^{-15}$ g/g with allowance for a uranium concentration of $(3–4) \cdot 10^{-8}$ g/g.

Searches for superheavy elements in other natural samples were made by the method of identifying events on the basis of tracks of two correlated fission fragments detected in two or three polymeric nuclear track detectors[161] with a film of the investigated material placed between them. One of the films (thickness about 12 μm) was scanned by the spark method.[160] The search for the track of the correlated fragment was made under a microscope after ordinary chemical etching of the detecting material. The coincidence method reduced the background appreciably and made it possible during a 10-month exposure to the Allende meteorite (~ 800 g) to observe just six fission events on an area of about 100 m^2 of detecting material [0.02 decays/(day·kg)]. This corresponded to a concentration of a spontaneously fissioning element of about 10^{-14} g/g with allowance for a uranium concentration $(1.5–2) \cdot 10^{-8}$ g/g and agreed with data obtained earlier by electronic methods.[154] This method can also be used in other investigations to determine extremely low concentrations of spontaneously fissioning impurities in various materials with sensitivity around 10^{-15} g/g.

To look for tracks made by extraterrestrial superheavy elements, meteoritic olivines were investigated in the studies of Refs. 162 and 163. The annealing method was used. Examination of the annealed olivine crystals revealed very long tracks (up to 365 μm), which may have corresponded to nuclei of superheavy elements ($Z > 110$). However, a more careful calibration of the olivines using large-Z ions is required if a reliable conclusion is to be drawn.[164]

More detailed reviews of searches for superheavy elements using SSNTDs can be found in Refs. 154, 165, and 166.

Investigation of the mechanisms and products of nuclear reactions by means of SSNTDs

Investigations of the mechanisms and products of nuclear reactions by means of SSNTDs reduce to identification of the products in the exit channel with respect to Z and A, the determination of their half-lives, and measurement of the angular and energy distributions as functions of the energy and species of bombarding particles and targets.

The choice of the detector and of the irradiation geometry depends on the aim of the experiment and on the detection properties of the SSNTDs. As a rule, an external target is used, though sometimes SSNTDs are also used as targets, in which case one investigates tracks that cross the surface, or one uses special methods to identify events within a layer of the detectors.[167,168]

Induced fission

The high efficiency of fission-fragment detection by SSNTDs, the threshold sensitivity, the possibility of adjusting this sensitivity, the low intrinsic background of SSNTDs, and the use of 2π and 4π irradiation geometries made possible a great variety of fission studies (Refs. 5, 8, 38, 169, and 170). The possibility of using large areas, and of different shapes, makes it possible to detect very low fission-fragment fluxes.

Generally, two irradiation geometries are used. In the first, the detector is placed immediately next to the target, or a thin layer of the material is placed between two plates of detectors. In this case, the number of reaction products is integrated over all emission angles. In the second geometry, the detector is at a certain distance, and information is gathered by measuring the dependence of the track density on the detector position.

It is possible to introduce material directly into a detecting material, for example, phosphate glass,[171] without changing its detection properties.

Solid-state nuclear track detectors have been used to measure low fission cross sections (down to 10^{-34}–10^{-36} cm^2),[172,173] to measure the angular distribution of fission fragments,[174,175] to determine fission barriers,[8,176] and to study double and triple fission induced by charged particles, neutrons, and γ rays.[5,177] Such detectors are also suitable for detecting events with low probability, for example, multifragment fission, which is difficult to detect by electronic counters. At the same time, the SSNTD method

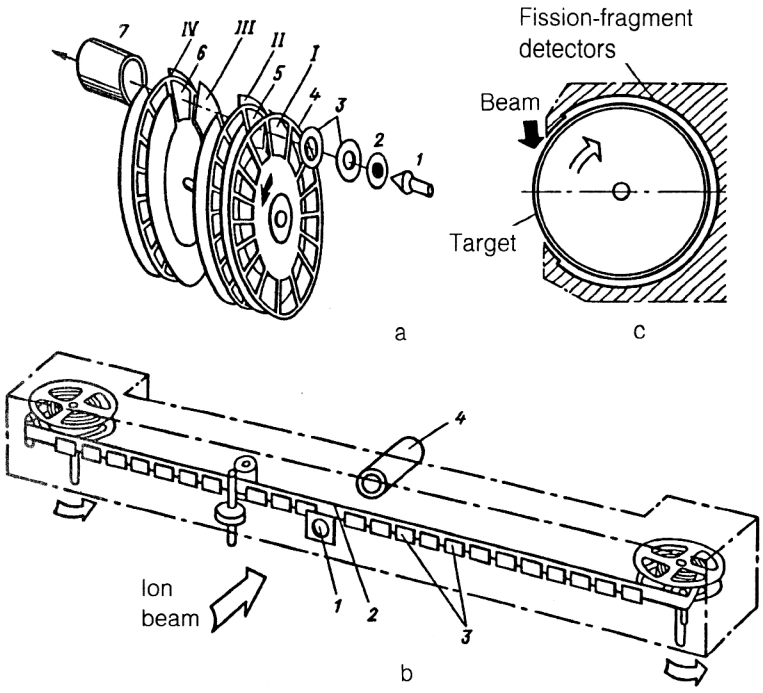

FIG. 29. Schematic arrangement of facilities for obtaining compound nuclei and studying their spontaneous fission by SSNTDs:[183] a) the facility Diski: 1) ion beam; 2) target; 3) collimators of recoil nuclei; 4) "mask" disk; 5) first collector disk of recoil nuclei; 6) second collector disk of recoil nuclei; 7) Faraday cylinder connected to current integrator; I–IV denote fission-fragment track detectors; b) scheme of facility with a long tape ($\sim$800 m) to transport synthesized nuclei to the SSNTD: 1) target; 2) metallic collector tape; 3) SSNTD; 4) Faraday cylinder; c) facility for detection of short-lived spontaneously fissioning nuclei.

makes it possible to calculate the corresponding cross section, and measurement of the range makes it possible to identify the fission products and to establish event coplanarity.

The results of studies of double and triple fission of Au, Bi, Ag, and U nuclei induced by protons, antiprotons, pions, α particles, and nitrogen ions at high energies using mica and polycarbonate detectors are given in Refs. 171 and 176–181. Phosphate glasses containing 2–3% of U, Th, and Bi were used to investigate fission induced by 18-GeV protons. The triple-fission threshold was established; it is situated in the region 0.5–0.7 GeV for protons.[176–180] Fission induced by high-energy protons[178] and α particles[170] has been investigated by a sandwich technique.

If heavy ions are used, it is expedient to operate in 2π geometry,[169,181] since the fission fragments are emitted in the forward hemisphere on account of the large momentum transfer from the heavy bombarding particle to the compound nucleus. To this end, thin films of fissioning materials [$\sim$1 mg/cm^2 of UF_4, ThF_4, Bi, Pb, and Au (Refs. 169 and 178)] were deposited by vaporization on mica detectors (areas between 1 and 10 cm^2) and irradiated with heavy ions: Kr, Xe, Pb, and U ($\sim 10^6$ ion/cm^2) with energy from 1 to 2 GeV.[182–193] After etching, an investigation was made of correlated events having extended tracks and reliably distinguishable from the tracks of ions entering at 90° and having the form of small rhombohedra. Measurement of the track length and angles of entry and exit of the fragments made it possible to identify the fragments and to obtain the total kinetic energy and the angular distribution of elastically scattered ions. A count of the ion tracks made it possible to determine the integrated flux of ions through the detectors and to calculate the reaction cross section. Five-prong events were observed in the interaction of U with U nuclei at energy 2 GeV.[193] Kinematic analysis of these events showed that they arose as a result of cascade fission.[186]

An interesting experiment is the measurement of the number $\bar{\nu}$ (the mean number of neutrons per fission event) for fission of the heavy nuclei of gold, bismuth, and uranium induced by carbon, oxygen, and neon ions. In the experiment of Ref. 194, in which a target was irradiated with a beam of heavy ions, the number and angular distribution of the neutrons, and also the number of fragments from the target were measured simultaneously. The neutrons were detected by glasses in contact with the fissioning material, which was neptunium-237. Fragments were also detected by glass SSNTDs. It was found that $\bar{\nu}$ depended strongly on the excitation energy of the fissioning nucleus. This method was also used to measure the angular distributions of neutrons produced by irradiation of Ge, Mo, Ag, and Pr targets with C, O, Ne, and Ar heavy ions.[195]

It should be noted that most studies of fission from isomer states have been made by means of SSNTDs (Refs. 8, 97, and 196–198). Isomer states were found for the nuclei of U, Np, Pu, Am, Cm, and Bk with half-lives $10^{-3} \geqslant T_{1/2} \geqslant 10^{-11}$ sec and cross sections down to $\sim 10^{-30}$ cm^2.

Study of mechanisms of formation and decay of compound nuclei

Transfermium elements are synthesized as a result of complete fusion of a bombarding particle with a target nucleus.[199] The production of a new element is a very rare process and has a cross section $\leqslant 10^{-34}$ cm^2. One requires long irradiation (up to several days) with intense beams up to $\sim 10^{18}$ cm^{-2}. The half-lives of these nuclei are short ($\leqslant 10^{-3}$ sec), and therefore they must be brought to the detectors extremely rapidly. The direction of emission of

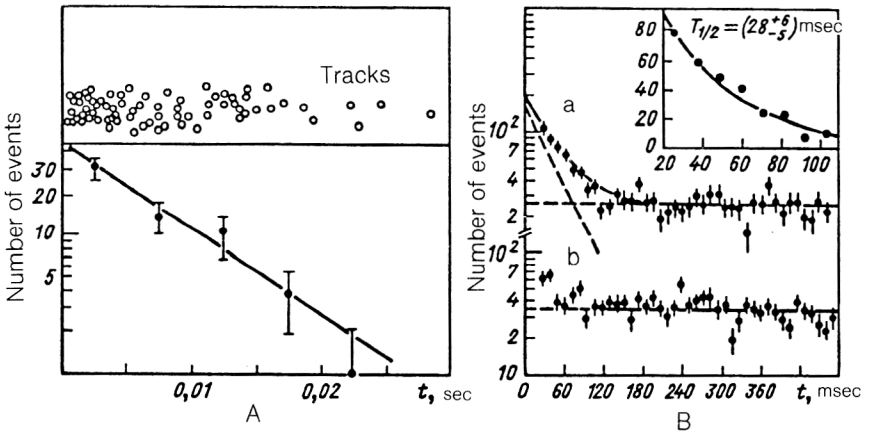

FIG. 30. Time distribution of tracks of fragments of spontaneously fissioning nuclei: A) obtained in the $^{208}Pb+^{50}Ti$ reaction using the facility of Fig. 29c; B) obtained in the $^{249}Bk+^{15}N$ reaction using the facility of Fig. 29a [a) for collector 5; b) for collector 6].

the recoil nuclei from the target coincides with the direction of the ion beam. Compound nuclei with half-lives $\geqslant 10^{-4}$ sec are removed from the region of the beam mechanically, being knocked into a rotating or moving collector (which transports the nuclei to the detectors by mechanical transport of the recoil atoms), by means of gas flows, or by electric and magnetic fields of separators.[73–75] The last method makes it possible to study nuclei with half-lives down to 10^{-7} sec. The decay of nuclei with half-lives $< 10^{-7}$ sec can be detected in flight after their emission from the target.[5] Use is made here of the noncoincidence of the angles of emission of the decay products and the beam direction. The half-lives of compound nuclei in the range 10^{-16}–10^{-19} sec are measured using irradiation of single-crystal targets ("shadow method").

Two forms of radioactivity are characteristic of transfermium elements: α decay and spontaneous fission. At Dubna, compound nuclei were detected by SSNTDs mainly through their spontaneous fission.[199] The reaction products were transported to the detectors by taking the collectors of the nuclei from the target to the detectors.[130] Figure 29 shows schematically the facilities most often used at the JINR to obtain compound nuclei and study their decay. In the first two schemes, the target is irradiated with an extracted ion beam (Figs. 29a and 29b),[200,201] while the third arrangement is designed for work using the internal beam of the accelerator to obtain maximum beam intensity of the accelerated ions.[202] The collectors of the nuclei are moved at speeds up to 10^3–10^4 mm/min. The half-lives were obtained from the distribution of the tracks in the detectors with respect to the direction of motion of the collector (Fig. 30). A long length of tape successfully solved the problem of suppressing the background from long-lived products.[203] The efficiency of detection of fission fragments of the studied nuclei achieved in these facilities was $\sim 65\%$.

Kinematic separators[73–75,204] made it possible to study spontaneous fission and α decay in the focal plane by means of SSNTDs.

For detection of fission fragments with different Z of the ions, muscovite mica, phosphate glass, polyethylene terephthalate, and polycarbonate have been used. Alpha-active nuclei have been studied using poly-allyl-glycol-carbonate.[136]

Because the irradiation process generates high neutron flux densities (10^{11}–10^{13} cm^{-2}), particular attention was devoted to the intrinsic background of the SSNTDs and of the construction materials (Table V). The background of tracks of scattered ions near the target had a flux density greater than 10^6 cm^{-2}. Therefore, in experiments using beams of ions with $Z \leqslant 10$ inorganic SSNTDs were employed,[47,200] and for ions with $Z \leqslant 15$, up to Fe, controlled selective annealing was used to reduce the background; as was shown in Sec. 3, this lowered the sensitivity to ions but maintained high detection efficiency for fission fragments (see Fig. 11). As an example illustrating the possibilities of this method, Fig. 31 shows microphotographs of the tracks of scattered chromium ions and a fission fragment of a nucleus obtained in the $^{207}Pb+^{54}Cr$ reaction before and after annealing of the detecting material.[47,130] The changes in the etchability of the tracks in polymeric SSNTDs resulting from the absence of oxygen during operation in vacuum and at high temperature were

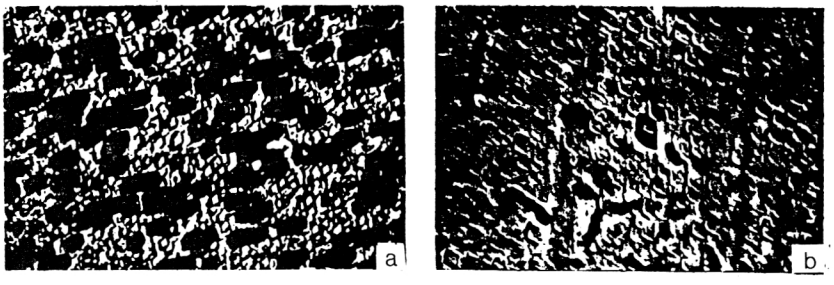

FIG. 31. Microphotographs of tracks of scattered ^{54}Cr ions and a track of a fission fragment of a nucleus obtained in the $^{207}Pb+^{54}Cr$ reaction before annealing (a) and after annealing at 460 °C for 6 h (b).

restored by irradiation with ultraviolet light with wavelength $\geqslant 310$ nm.

Inorganic nuclear track detectors permit detection of spontaneous fission at high temperatures. In experiments using chemical identification of kurchatovium and nielsbohrium and a study of their properties, fragments were detected in muscovite mica at temperatures up to 400 °C in an atmosphere of volatile chlorides.[205] None of the known electronic counters can operate under such conditions.

For additional identification of tracks of fission fragments from background events (in the facility shown in Fig. 29a) tracks of paired fission fragments were correlated in two opposing SSNTDs based on the two sides of a thin collector of nuclei. Coincidence of oppositely directed fragment tracks indicated the decay of a spontaneously fissioning nucleus and made it possible to separate fragments from background ions with $Z \geqslant 26$, whose tracks cannot be annealed.

Compound nuclei and decay products were identified on the basis of the range or diameter of their tracks in SSNTDs (see Sec. 3). Differences between the total kinetic energies of the fission fragments made it possible to distinguish fragments of spontaneously fissioning products of transfer reactions (for example, ^{241}Am nuclei in an isomer state, ^{256}Fm isotopes, etc.) from fission fragments of compound nuclei, which, as a rule, have higher total kinetic energies. If separators are used, SSNTDs can detect both the compound nucleus itself and the fission fragments and α particles emitted from it (Fig. 32). Measurement of the ranges gives a complete energy picture of the decay, permitting event identification (see Sec. 3).

Solid-state nuclear track detectors have been used to study many (more than 100) nuclear synthesis reactions in beams of heavy ions with $Z=2$–36 for a large range of targets with $Z=70$–98. Nuclei with atomic numbers 102–104 have been investigated by means of radioactive targets.[200] In cold-fusion reactions,[202] in which Ta, Pb, and Bi isotopes were irradiated with ions from Ar to Fe, the stability of transfermium elements with $Z=104$–110 was investigated (Fig. 33). The use of SSNTDs made it possible to study[199] nuclear reactions with a cross section of about 10^{-36} cm^{-2}.

To detect spontaneously fissioning nuclei with half-lives less than 10^{-6} sec, the method shown schematically in Fig. 34a was used.[196] The SSNTDs detected fission fragments of recoil nuclei that decayed in flight. By means of glass and mica detectors, it was possible to measure the cross sections of the reactions ^{238}U(^{12}C, $4n$) (Ref. 206), ^{238}U(n, n'), ^{239}Pu(n, n'), ^{242}Pu(n, n'), and ^{242}Pu(n, $2n$), which lead to production of spontaneously fissioning isomers with half-lives 10^{-6}–10^{-9} sec.[207] Since the velocity of the recoil nuclei produced in reactions with light ions is $(0.2$–$0.6)\cdot 10^8$ cm/sec, direct use of this method limits the half-life that can be measured to a few nanoseconds. A further development of this method was the so-called projection method,[172] the principle of which is shown in Fig. 34b. A target of radius $\rho \leqslant 1$ mm is bombarded with a beam of ions. The tube in which the target is fixed has radius r. The fission-fragment detectors are mounted on a cylinder

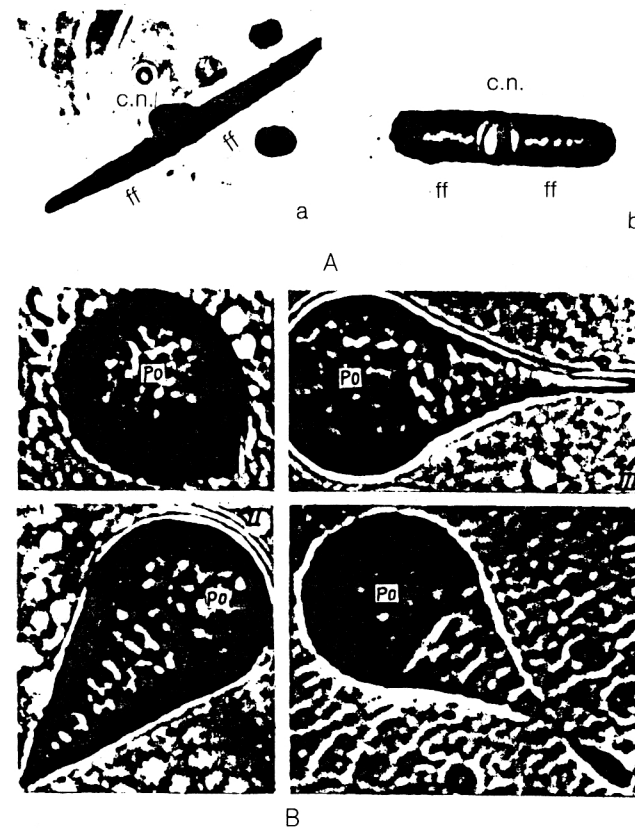

FIG. 32. Microphotographs of tracks of compound nuclei (c.n.) ^{244}Fm (A) entering PETP at 45° (a) and 90° (b) to the surface of the SSNTD, tracks of paired fission fragments of this nucleus (ff) and Po nuclei (B) (disk) entering PAGC perpendicularly, and the tracks of α particles emitted from these Po nuclei at various angles to the surface of the SSNTD.

at distance R from the beam axis. In this case, a recoil atom at distance x from the target emits, on decay, fragments that can be detected over a length $l=(R-r)x/r$ of the detector. Estimates show that by means of the projection method it is possible to measure the half-lives of spontaneously fissioning isomers down to $5\cdot 10^{-12}$ sec. Indeed, a spontaneously fissioning ^{240}Cm isomer with $T_{1/2}=10^{-11}$ sec was obtained in Ref. 208.

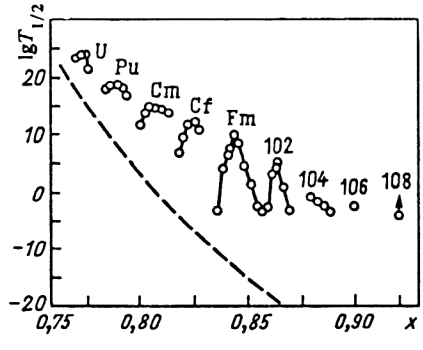

FIG. 33. Half-lives of transuranium nuclei as functions of the fissility parameter x.[201]

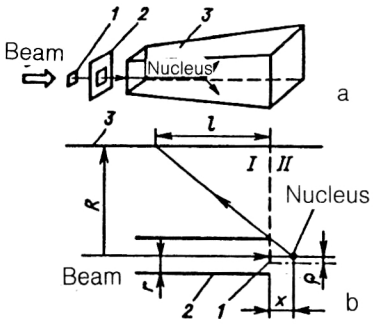

FIG. 34. Detection of the decay of spontaneously fissioning nuclei in flight (Refs. 73, 207, and 208): a) for the range of half-lives 10^{-7}–10^{-9} sec: 1) target; 2) collimator; 3) glass detectors; b) for times down to 10^{-12} sec: 1) target; 2) tube for fixing target; 3) solid-state detectors of fission fragments; I) zone of detection of fragments of delayed fission; II) zone of detection of fragments of induced fission.

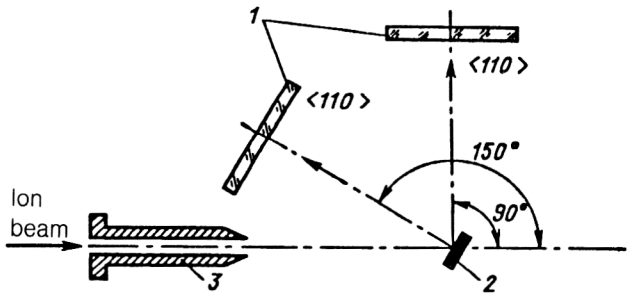

FIG. 35. Schematic arrangement of an experiment to determine half-lives of compound nuclei by means of the shadow effect: 1) fission-fragment detectors; 2) single crystal; 3) collimator.

There is great interest in the use of different types of SSNTD to measure half-lives of compound nuclei in the range 10^{-15}–10^{-18} sec by a method based on observation of a shadow effect in the angular distributions of the products of nuclear reactions in a single-crystal target.[209] Under the influence of the momentum of the bombarding particle, the compound nucleus is displaced from its lattice site. At the time of decay, the compound nucleus is on the average a distance $S=v\tau$, where v is the velocity of the nucleus and τ is the mean lifetime of the nucleus, from the site. Charged particles emitted by nuclei at the sites of a crystal lattice in the directions of the crystal axes and planes are subject to strong scattering already by the nearest nuclei. In the angular distributions of the particles that leave the crystal, there are regions with sharply reduced particle intensity, i.e., "shadows," the positions of which are determined by the structure of the crystal. Displacement of nuclei from sites leads to changes in the shapes of the shadows in the angular distributions of the decay products, from which, for a known velocity of the recoil nucleus, the value of τ can be determined. For measurement of half-lives by this method, a collimated beam of bombarding particles is directed onto a single crystal containing atoms of the investigated fissioning element at an angle which ensures that images of the reference and working shadow pictures are obtained simultaneously in the SSNTDs (at 90 and 150°, respectively, with respect to the ^{22}Ne ion beam; Fig. 35). After appropriate treatment of the detectors, the tracks in the regions of the shadows formed along the principal crystallographic axes are counted, the "depths" of the reference and working shadows are compared, and conclusions are drawn about the lifetime of the compound nucleus. This method was used to measure the half-lives of excited states of nuclei using irradiation of single-crystal targets of ^{186}W, ^{181}Ta, ^{238}U, etc., with ^{11}B, ^{12}C, ^{16}O, ^{20,22}Ne, ^{27}Al, and ^{31}P ions with different energies; information was also obtained about the mechanism of emission of α particles in ^{20}Ne, ^{40}Ar+Ge reactions using cellulose nitrate SSNTDs.[210] In these last experiments, the SSNTDs can be used not only as position-sensitive but also as spectrometric detectors. For each detection angle, a set of filters of different thicknesses were used in front of the detector. In one irradiation, with low exposures, the spectral and angular distribution of α particles was obtained. The use of a pile of thin SSNTDs instead of foil can give more detailed information. More complete data about this method and the results of investigations are given in the review of Ref. 209.

The use of SSNTDs in such investigations makes it possible to cover in a single experiment a wide range of angles and to investigate interactions that take place with low cross sections. Thus, to study the fission barriers of ^{230}Th and ^{231}Pa in the (n, f) reaction, a large scattering chamber was used in order to obtain adequate statistics.[211] Polycarbonate of area $\sim 5\cdot 10^4$ cm^2 was used to determine the cross section of below-barrier fission and the angular distribution of fragments of induced fission of ^{230}Th and ^{231}Pa at neutron energies 690–740 and 160 keV, respectively. In the study of Ref. 212, polycarbonate detectors were used to measure the angular distributions of two groups of α particles produced on the production of ^{24}Mg in the ground state and in an excited state in the ^{27}Al(p, d) reaction. The α particles were distinguished by measuring the track diameters, and an energy resolution of about 60 keV at $\sim$6 MeV was obtained.

Study of the ^{12}C(^{12}C, ^{8}Be) ^{16}O and ^{10}B(p, α) ^{7}Be reactions at low energies of the incident particle is of astrophysical interest. The use of a definite type of polycarbonate detector (insensitive to protons) made it possible[213,214] to determine reliably the reaction cross section and to measure the angular distribution of the reaction products despite a large background of elastically scattered ions and protons, which would have been difficult to achieve by electronic methods.

A large series of investigations of the interaction of accelerated ^{238}U, ^{208}Pb, and ^{139}La heavy ions with energies $\geqslant$10 MeV/amu with ^{108}Ag, ^{165}Ho, ^{189}W, ^{197}Au, and ^{209}Bi nuclei was made in Refs. 215 and 219. An SSNTD pile, on each layer of which a film of the target material was deposited, was used. Measurement of the total range and angles of correlated events made it possible to analyze the angular distribution of elastically scattered ions and interaction products.

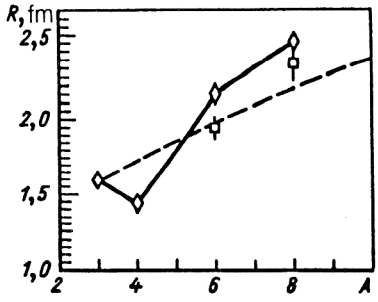

FIG. 36. Radii of He isotopes as functions of the mass number: the diamonds are the results of Ref. 221, and the squares are the results of Ref. 143.

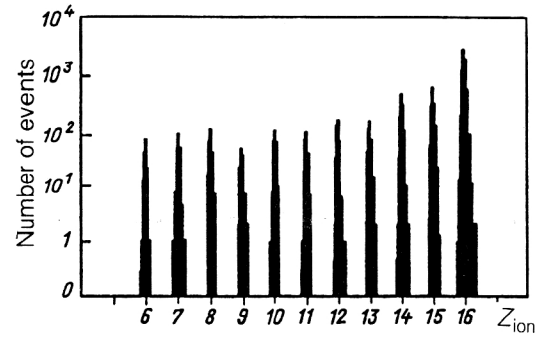

FIG. 37. Charge distribution of fragments resulting from interactions with PAGC of ^{16}O with $E=200$ GeV/amu, obtained by measuring the track diameters in 30 films of a pile of 150 films.

Elastic scattering of charged particles

In various centers, work has recently begun on the use of secondary radioactive beams formed from radioactive products of nuclear reactions in order to obtain information about the structure of nuclei far from the stability region, namely, about the distribution of nuclear matter or nuclear radii.[220] To this end, one measures the interaction cross sections of these nuclei with target nuclei or the elastic scattering of radioactive ions. As yet, the intensities of the secondary beams are low (about 10^3 particles/sec was obtained with the U-400 accelerator at Dubna; in France, $\sim 10^6$ particles/sec was obtained with the accelerator GANIL), and if electronic methods are used, long exposures are needed. In this case, SSNTDs, by virtue of their size, make it possible to obtain adequate statistics for measurement of elastic scattering in a wide range of angles. Elastic scattering of ^{6}He, ^{8}He, ^{8}Li, and ^{9}Li by C, Be, Ta, and Ag nuclei was investigated in Ref. 143. A pile of two PAGC films was used. The isotopes were identified by measuring the track diameters of the ions and their variation along the particle trajectories. Figure 25 shows calibration distributions of the diameters of ^{4}He, ^{6}He, ^{8}He, and ^{9}Li tracks with energies 57, 43, 94, and 86 MeV. The dependence of the values found for the radii of He isotopes on the mass number is shown in Fig. 36. The data correlate well with the results of Ref. 221, which were obtained by electronic methods.

Multiparticle processes

If SSNTDs are used to investigate nucleus–nucleus reactions at intermediate and high energies, it is possible, in a simple and economic manner, to measure, in 2π and 4π geometries, fragmentation both of the target and of the incident ions and to separate the different reaction channels. The emission in different phases of the interaction can be determined: direct emission in the first phase of the interaction (like the lightest fragments in multifragmentation) and evaporation from heavier fragments in the second phase. Many studies have been made using ions from ^{4}He to ^{238}U with energies from several mega-electron-volts to several hundred giga-electron-volts with targets from nuclei of hydrogen, carbon, and oxygen contained in the SSNTDs themselves to uranium nuclei. The results of these investigations are presented in Refs. 169 and 222–230.

Depending on the energy of the incident ions, various methods have been used to identify fragments. In the study of Ref. 222, in which the total length of the etched track of fragments and the etching selectivity were measured, the charge resolution achieved in PAGC was $\Delta Z \leqslant 1$ for nuclei with $Z < 30$, $\Delta Z \leqslant 2$ for nuclei with $Z > 30$ and $E/A > 0.5$ MeV, and $\Delta Z \leqslant 4$ for nuclei with $E/A \leqslant 0.5$ MeV. For 10 MeV/amu of nuclei with $Z \sim 80$, the resolution achieved by this method was $\Delta Z = 2$. The energy resolution for the observed reaction products was $\Delta(E/A) \leqslant 0.05$ MeV, and the maximum error in the determination of the angle was 5°. For the interval of energies from 10 to 20 MeV/amu, a resolution $\Delta Z < 1$ was achieved in measurement of the pits of multiply etched tracks.[231] A charge resolution of $0.027e$ was obtained by irradiating CH_2, C, CR-39, Al, Cu, Ag, and Pb with various ions of energies from 0.6 to 200 GeV/amu and using a computer technique for scanning and analysis of the experimental data. The resolution was achieved by the $D(R_{res})$ method by measuring the track diameters in 100 detecting surfaces of a pile irradiated with ^{16}O ions (200 GeV/amu). As an example, Fig. 37 shows the charge distribution of the products of ^{16}O interactions with the detector material. The resolution achieved was $0.05e$ on the basis of measurement of track diameters in 30 films of a pile made of 150 films. Using a large SSNTD pile (polycarbonate) in the focal plane of a magnetic spectrometer and measuring the range, angular distribution, and v_t/v_m, the authors of Ref. 232 succeeded in determining the Z, A, and M values of fragments, and they discovered two neutron-enriched nuclides ^{20}C and ^{27}F in the ^{48}Ca+Be reaction. Besides the experiments discussed above, SSNTDs have been used in experiments to look for anomalous nuclei (anomalons) formed in nuclear reactions and possessing fractional charge and large radii.[233] However, these investigations have not yet given reliable results that confirm the existence of such nuclei.

Solid-state nuclear track detectors are also widely used in different fields, for example, to study the composition of cosmic rays at various heights and latitudes of the

magnetosphere,[72,234–237] solar activity,[72,233–235] galactic radiation,[238] to look for Dirac monopoles,[239] to determine the age of samples,[8,38,240] in radiography,[8,38,241,242] in dosimetric measurements of the fluxes of neutrons and charged particles,[243] to prepare filtering matrices with given pore diameters (Refs. 8, 38, 47, 89, and 244), and in other applied investigations.[245,246]

[1] E. C. H. Silk and R. S. Barnes, Philos. Mag. **4**, 970 (1959).
[2] G. Somogyi, M. Toth-Szilagyi, M. Monin *et al.*, in *Proc. of the Tenth Intern. Conf. on Solid State Nuclear Track Detectors* (Pergamon Press, Oxford, 1980), p. 267.
[3] D. A. Young, Nature **182**, 375 (1958).
[4] P. B. Price and R. M. Walker, J. Appl. Phys. **33**, 3400 (1962).
[5] Yu. P. Gangrskiĭ, B. N. Markov, and V. P. Perelygin, *Detection and Spectrometry of Fission Fragments* [in Russian] (Énergoizdat, Moscow, 1981).
[6] S. Lindhard, M. Scharff, and H. E. Schiott, K. Dan. Vidensk. Selsk. Mat.-Fys. Medd. **33**, 1 (1965).
[7] H. A. Bethe, Ann. Phys. (N.Y.) **5**, 325 (1930).
[8] R. L. Fleischer, P. B. Price, and R. M. Walker, *Nuclear Tracks in Solids: Principles and Applications* (University of California Press, Berkeley, 1975).
[9] F. Bloch, Z. Phys. No. 1, 363 (1933).
[10] R. Katz and E. J. Kobetich, Phys. Rev. **170**, 391, 401 (1968).
[11] R. Katz, Nucl. Tracks **8**, 1 (1984).
[12] S. Fain, M. Monnin, and M. Montret, Radiat. Res. **57**, 379 (1974).
[13] E. V. Benton, Report USNRDL-TR-67-80, San Francisco (1967).
[14] E. V. Benton and W. D. Nix, Nucl. Instrum. Methods **67**, 343 (1969).
[15] E. V. Benton, Radiat. Eff. **2**, 273 (1970).
[16] L. C. Northcliffe and R. F. Schilling, Nucl. Data Tables **A7**, 233 (1970).
[17] H. Geissel, P. Armbruster, T. Kitohara *et al.*, Nucl. Instrum. Methods **170**, 217 (1980).
[18] Gy. Almasi and G. Somogui, ATOMKI Kosl. **23**, 99 (1981).
[19] G. Pretzch, TU-Information 05-01-79, Dresden (1979).
[20] T. Noggle and L. Stigler, J. Appl. Phys. **31**, 1259 (1959).
[21] N. F. Pravdiuk and V. M. Goljanov, *Radiation Damage in Solids* (IAEA, Vienna, 1962), p. 333.
[22] S. C. Vareille, S. L. Decossas, S. P. Moliton *et al.*, J. Polym. Sci. **20**, 1327 (1982).
[23] D. V. Morgan and L. T. Chadderton, Philos. Mag. **17**, 1335 (1968).
[24] D. Albrecht, P. Ambruster, R. Spohr *et al.*, Radiat. Eff. **65**, 145 (1982).
[25] M. Lambert, Radiat. Eff. **3**, 155 (1970).
[26] S. L. Teysaier, S. L. Docossas, and J. C. Vareille, Nucl. Tracks **12**, 26 (1986).
[27] S. P. Moliton, C. Boevtinaud, and A. Decossas, Polym. Sci.: Polym. Phys. Ed. **20**, 1280 (1982).
[28] A. Chambaudet and P. Romary, in *Proc. of the Tenth Intern. Conf. on Solid State Nuclear Track Detectors* (Pergamon Press, Oxford, 1980), p. 35.
[29] V. I. Popov, *Methods of Linear Energy Loss Spectrometry of Ionizing Radiations* [in Russian] (Atomizdat, Moscow, 1978).
[30] R. A. Edmonds and S. A. Durrani, Nucl. Tracks No. 3, 3 (1979).
[31] W. T. Crawford, W. Desorbo, and J. S. Humphreys, Nature **220**, 1313 (1968).
[32] C. P. Bean, M. V. Doyle, and G. Entine, J. Appl. Phys. **41**, 1454 (1970).
[33] P. Yu. Apel' and S. P. Tret'yakova, Prib. Tekh. Eksp. **3**, 58 (1980).
[34] P. Yu. Apel and G. Pretzsch, Nucl. Tracks **11**, 45 (1986).
[35] Ya. E. Geguzin, I. V. Vorob'eva, and I. G. Berezina, Fiz. Tverd. Tela (Leningrad) **10**, 1819 (1968) [Sov. Phys. Solid State **10**, 1431 (1968)].
[36] E. Dortyge, J. Phys. **39**, 1287 (1978).
[37] R. Gold, S. H. Roberts, and F. H. Ruddy, Nucl. Tracks **5**, 253 (1981).
[38] S. A. Durrani and R. K. Bull, *Solid State Nuclear Track Detectors: Principles, Methods and Applications* (Pergamon Press, Oxford, 1987) [Russ. transl., Énergoatomizdat, Moscow, 1990].
[39] J. E. Griffith, T. A. Weller, L. E. Seiberling *et al.*, Radiat. Eff. **51**, 223 (1980).
[40] J. H. Varley, Nature **174**, 886 (1954).
[41] S. V. Starodubtsev and A. E. Kiev, Izv. Akad. Nauk Uzb. SSR, Ser. Fiz.-Mat. Nauk **3**, 41 (1963).
[42] R. M. Fleischer, in *Progress in Material Science* (Chalmers Anniversary Volume) (Pergamon Press, New York, 1980), p. 97.
[43] Ya. E. Geguzin and I. V. Vorob'eva, Fiz. Tverd. Tela No. 4, 927 (1980).
[44] D. O'Sillivan, P. B. Price, and K. Kinoshita, J. Electrochem. Soc. **129**, 811 (1982).
[45] P. B. Price, Philos. Mag. **45**, 331 (1982).
[46] D. O'Sillivan and A. Thompson, Nucl. Tracks No. 4, 271 (1980).
[47] S. P. Tret'yakova, "Solid-state nuclear track detectors and their use in experimental nuclear physics," Doctoral Dissertation [in Russian], JINR, Dubna (1989).
[48] F. A. Bovey, *The Effects of Ionizing Radiations on Natural and Synthetic High Polymers* (Interscience, New York, 1958).
[49] A. Charlesby, *Atomic Radiation and Polymers* (Pergamon Press, London, 1960).
[50] S. P. Tretyakova, P. Yu. Apel, L. V. Jolos *et al.*, in *Proc. of the Tenth Intern. Conf. on Solid State Nuclear Track Detectors* (Pergamon Press, Oxford, 1980), p. 283.
[51] N. S. Moshkovskiĭ, L. I. Gaĭchenko, and Ya. I. Lavrentovich, At. Energ. **42**, 104 (1977).
[52] P. Yu. Apel' and L. I. Kravets, Preprint 12-89-742 [in Russian], JINR, Dubna (1989).
[53] M. I. Chipara, T. Bunget, and R. Georgescu, Nucl. Instrum. Methods **209/210**, 395 (1983).
[54] S. P. Kapchigaev, V. N. Koval', V. A. Sokolov *et al.*, in *Problems of Dosimetry*, No. 2 [in Russian] (Atomizdat, Moscow, 1979), p. 57.
[55] A. Chambaudet and T. Roncin, Nucl. Tracks Suppl. No. 3, 15 (1982).
[56] H. B. Lück, Nucl. Instrum. Methods **114**, 139 (1974).
[57] Ya. M. Beprik, V. P. Romanenko, and S. P. Tret'yakova, Tr. Leningr. Inst. Kinoinzh. No. 19, 68 (1967); No. 22, 70 (1972); No. 23, 130 (1973); No. 26, 145 (1975); No. 32, 70 (1978).
[58] H. B. Lück, Nucl. Instrum. Methods **200**, 517 (1982); **213**, 507 (1983).
[59] Kristic, R. Anatanasijevic, and Z. Todorovic, Nucl. Tracks **7**, 147 (1983).
[60] J. Stejny and T. Portwood, Nucl. Tracks **12**, 121 (1986).
[61] A. Bernas, A. Chambaudet, and E. Bartgge, in *Proc. of the Eighth Intern. Conf. on SSDT, Bucharest, 1972* (IFA, Bucharest, 1972), p. 300.
[62] T. Portwood and J. Stejny, Nucl. Tracks **12**, 113 (1986); **8**, 151 (1984).
[63] T. Portwood, T. W. Turner, and A. P. Fews, Nucl. Tracks **8**, 155 (1984).
[64] B. G. Cartwright, E. K. Shirk, and P. B. Price, Nucl. Instrum. Methods **153**, 457 (1978).
[65] V. E. Kapchenov and V. A. Nicolaev, Nucl. Tracks Rad. Meas. **11**, 221 (1986).
[66] S. Aschenbach, G. Fiedler *et al.*, Nucl. Instrum. Methods **116**, 395 (1974).
[67] S. Wang, D. Barwick, D. Ifft *et al.*, Nucl. Instrum. Methods **B35**, 43 (1988).
[68] I. I. Berzina and I. V. Berman, Dokl. Akad. Nauk SSSR **172**, No. 3, 553 (1967) [Sov. Phys. Dokl. **12**, 275 (1967)].
[69] A. D. Belyaev, I. I. Bahromi, N. V. Beresina *et al.*, Nucl. Tracks **4**, 49 (1980).
[70] G. W. Dorling, R. K. Bull, S. A. Durrani *et al.*, Radiat. Eff. No. 23, 141 (1974).
[71] M. Begalli, A. Margues, and D. A. B. Serra, Nucl. Tracks **9**, 123 (1984).
[72] A. N. Marennyĭ, *Solid-State Nuclear Track Detectors in Radiation-Physics and Radiobiological Experiments* [in Russian] (Énergoatomizdat, Moscow, 1987).
[73] V. L. Mikheev, Fiz. Elem. Chastits At. Yadra **10**, 269 (1979) [Sov. J. Part. Nucl. **10**, 101 (1979)].
[74] V. Z. Maĭdikov, Yu. V. Gofman, G. S. Popeko *et al.*, Prib. Tekh. Eksp. No. 4, 68 (1979).
[75] Yu. Ts. Oganesyan, Yu. V. Lobanov, A. G. Popeko *et al.*, in *Abstracts of Papers of the International Seminar School on Heavy-Ion Physics, Dubna*, 1989, D7-89-531 [in Russian], JINR, Dubna (1989), p. 145.
[76] A. G. Belov, A. G. Bondarenko, and Ch. Shimane, Preprint R2-82-301 [in Russian], JINR, Dubna (1982).
[77] W. De Sorbo, Nucl. Tracks No. 3, 13 (1979).
[78] P. F. Green, A. G. Ramli, S. A. R. Al-Najjar *et al.*, Nucl. Instrum. Methods **203**, 551 (1982).
[79] G. Somogyi, Philos. Mag. **4**, 27 (1959).
[80] S. P. Tretyakova, P. Yu. Apel, L. V. Jolos *et al.*, in *Proc. of the Tenth*

Intern. Conf. on Solid State Nuclear Track Detectors (Pergamon Press, Oxford, 1980), p. 283.
[81] D. Hilderbrand and E. V. Benton, Nucl. Tracks **4**, 77 (1980).
[82] G. Somogyi and I. Hunyadi, in *Proc. of the Tenth Intern. Conf. on Solid State Nuclear Track Detectors* (Pergamon Press, Oxford, 1980), p. 443.
[83] W. Enge, K. Grabisch, L. Dallmeyer *et al.*, Nucl. Instrum. Methods **127**, 125 (1975).
[84] S. Singh, J. Singh, and H. S. Virk, Nucl. Tracks Rad. Meas. **15**, 187 (1988).
[85] R. P. Henke and E. V. Benton, Nucl. Instrum. Methods **97**, 483 (1971).
[86] G. Somogyi, Nucl. Instrum. Methods **173**, 21 (1980).
[87] A. Ali and S. A. Durrani, Nucl. Tracks Detection **1**, 107 (1977).
[88] G. Somogyi, R. Scherzer, K. Grabisch, and W. Enge, Nucl. Instrum. Methods **147**, 11 (1977).
[89] B. E. Fischer and R. Spohr, Rev. Mod. Phys. **55**, 907 (1983).
[90] R. Muhammed, F. Abu-Jarad, and M. T. Al-Jarallan, Nucl. Tracks **15**, 187 (1988).
[91] L. Tommasino, G. Zapparol, R. V. Griffith, and A. Mattei, Nucl. Tracks **4**, 191 (1980).
[92] G. Somogyi, Nucl. Track Detection No. 1, 3 (1977).
[93] S. P. Tret'yakova and L. V. Jolos, Prib. Tekh. Eksp. No. 3, 52 (1982).
[94] H. A. Khan, Radiat. Eff. No. 8, 135 (1971).
[95] G. M. Hassib, Nucl. Instrum. Methods **131**, 125 (1975).
[96] S. A. R. Al-Najjar, M. Balcazar-Carcia, and S. A. Durrani, Nucl. Track Detection No. 2, 215 (1978).
[97] S. P. Tret'yakova, "Development of methods of detection of heavy charged particles by means of nuclear emulsions and solid-state nuclear track detectors," Candidate's Dissertation [in Russian], JINR, Dubna (1968).
[98] W. G. Cross and L. Tommasino, Health Phys. No. 5, 196 (1968).
[99] L. Tommasino, N. Klein, and P. Solomon, Nucl. Track Detection No. 1, 63 (1977).
[100] A. Somogyi, I. Hunyadi, and Zs. Varga, Nucl. Track Detection No. 2, 191 (1978).
[101] A. Chambaudet, D. Fellmaun, M. Rebetez *et al.*, Nucl. Tracks **8**, 207 (1984).
[102] G. Somogyi, L. Medveczky, I. Hunyadi, and B. Nyako, in *Proc. of the Ninth Intern. Conf. on SSNTD*, Munich, 1976 (Pergamon Press, Oxford, 1978).
[103] S. A. R. Al-Najjar, R. K. Bull, and S. A. Durrani, in *Proc. of the Tenth Intern. Conf. on Solid State Nuclear Track Detectors* (Pergamon Press, Oxford, 1980), p. 323.
[104] V. I. Pribytnov and B. S. Rozov, Prib. Tekh. Eksp. No. 4, 7 (1975).
[105] R. Gold, J. H. Roberts, C. Preston *et al.*, Nucl. Tracks **8**, 187 (1984).
[106] A. Noll, G. Rusch, H. Rocher *et al.*, Nucl. Tracks **15**, 265 (1988).
[107] S. Dreute, W. Trakowski, B. Schofer *et al.*, Nucl. Tracks **12**, 261 (1986).
[108] G. Somogyi, K. Grabisch, R. Scherzer, and W. Enge, Nucl. Instrum. Methods **134**, 129 (1976).
[109] A. N. Golovchenko, L. V. Jolos, and S. P. Tret'yakov, in *Proceedings of the Working Symposium: Solid-State Nuclear Track Detectors and Their Application*, Dubna, 1990, D13-90-479 [in Russian], JINR, Dubna (1990), p. 53.
[110] H. B. Lück, in *Abstracts of the 15th Intern. Conf. on Particle Tracks in Solids*, Marburg, 1990 (Marburg, 1990), p. 94.
[111] O. Otgonsuren, V. P. Perelygin, and S. P. Tret'yakova, in *Proc. of the Eighth Intern. Conf. on SSDT*, Bucharest, 1972 (IFA, Bucharest, 1972), p. 231.
[112] Kh. Abdullaev, A. Kapustsik, O. Otgonsuren *et al.*, Prib. Tekh. Eksp. No. 2, 73 (1968).
[113] S. B. Homer and S. C. Miles, Nucl. Tracks **12**, 133 (1986).
[114] D. O'Sillivan, A. Thompson, S. A. Adams *et al.*, Nucl. Tracks **8**, 143 (1984); **4**, 271 (1980).
[115] S. H. Adams and L. P. Beahm, Nucl. Tracks **12**, 387 (1986).
[116] A. Kapuscik, V. P. Perelygin, S. P. Tretyakova *et al.*, in *Proc. of the Sixth Intern. Conf. on Nucl. Photography* (CEPI, Rome, 1966), p. 468.
[117] B. Jakupi, D. Lhagvasuren, O. Otgonsuren *et al.*, in *Proc. of the Tenth Intern. Conf. on Solid State Nucl. Track Detectors* (Pergamon Press, Oxford, 1980), p. 997.
[118] G. Singh and H. S. Virk, Nucl. Tracks Rad. Meas. **15**, 253 (1988).
[119] S. K. Modgil and H. S. Virk, Nucl. Instrum. Methods **B21**, 60 (1987).
[120] M. Zamani, E. Savvides, J. Petrakis *et al.*, Nucl. Tracks **12**, 141 (1986).
[121] H. B. Lück, Nucl. Instrum. Methods **212**, 371 (1983).
[122] B. Schlenk, G. Somogyi, and A. Valek, Radiat. Eff. No. 24, 24 (1975).
[123] S. A. Durrani and K. Iames, Nucl. Tracks Rad. Meas. **15**, 223 (1988).
[124] M. Zamani, S. Sampsonidis, and S. Charalambous, Nucl. Tracks **12**, 125 (1986).
[125] S. P. Tret'yakova and T. I. Mamonova, At. Energ. **47**, 216 (1979).
[126] T. Portwood and D. L. Hewshaw, Nucl. Tracks **12**, 105 (1986).
[127] K. Fukuda, H. Fujimoto, and Y. Satoh, Nucl. Instrum. Methods **251**, 374 (1986); **174**, 421 (1980).
[128] H. Khan and N. Khan, Nucl. Instrum. Methods **216**, 471 (1983).
[129] W. D. De Sorbo, Nucl. Tracks No. 3, 13 (1979).
[130] S. P. Tret'yakova and R. N. Sagaĭdak, *Autoradiographic Method in Scientific Investigations* [in Russian] (Nauka, Moscow, 1990).
[131] Csigel, I. Hunyadi, G. Somogyi *et al.*, Nucl. Tracks Rad. Meas. **15**, 179 (1988).
[132] V. P. Perelygin, S. G. Stetsenko, O. Otgonsuren *et al.*, Nucl. Tracks **12**, 375 (1986).
[133] R. N. Sagaidak and S. P. Tretyakova, Nucl. Tracks **12**, 317 (1986).
[134] K. Endo and T. Doke, Nucl. Instrum. Methods **111**, 29 (1973).
[135] S. K. Boeggild, O. H. Arroe, and T. Sigurgeirsson, Phys. Rev. **141**, 1146 (1966).
[136] S. P. Tret'yakova, A. V. Eremin, Yu. V. Lobanov, and T. V. Tetereva, in *Proceedings of the Working Symposium: Solid-State Nuclear Track Detectors and Their Applications*, Dubna, 1990, D13-90-479 [in Russian], JINR, Dubna (1990), p. 64.
[137] V. G. Bogdanov, N. P. Kocherov, and O. E. Shigaev, Prib. Tekh. Eksp. No. 3, 69 (1989).
[138] S. Grabez, R. Beckmann, P. Vater, and R. Brandt, Nucl. Tracks **12**, 769 (1986).
[139] V. G. Bogdanov, N. P. Kocherov, F. G. Lepekhin *et al.*, Pis'ma Zh. Eksp. Teor. Fiz. **44**, 306 (1986) [JETP Lett. **44**, 391 (1986)].
[140] G. Siegmon, H. J. Kohnew, D. P. Bartholoma, and W. Enge, in *Proc. of the Ninth Intern. Conf. on SSNTD*, Munich, 1976 (Pergamon Press, Oxford, 1978), p. 137.
[141] Z. Todorovich and R. Anatanasijevic, Nucl. Instrum. Methods **212**, 217 (1983).
[142] P. B. Price, Nucl. Phys. **A502**, 41 (1989).
[143] S. P. Tretyakova, C. Borcea, R. Kalpakchieva, Nucl. Instrum. Methods **224**, 371 (1984).
[144] H. K. Skobelev, S. M. Luk'yanov, and Yu. É, Penionzhkevich, Preprint R7-90-195 [in Russian], JINR, Dubna (1990).
[145] A. P. Fews and D. L. Henshaw, Nucl. Tracks **12**, 641 (1986).
[146] H. S. Rose and G. Jones, Nature **307**, 345 (1984).
[147] D. V. Aleksandrov, A. F. Belyatskiĭ, Yu. A. Glukhov *et al.*, Piz'ma Zh. Eksp. Teor. Fiz. **40**, 152 (1984) [JETP Lett. **40**, 909 (1984)].
[148] A. Săndulescu, D. N. Poenaru, and W. Greiner, Fiz. Elem. Chastits At. Yadra **11**, 1134 (1980) [Sov. J. Part. Nucl. **11**, 528 (1980)].
[149] Yu. S. Zamyatin, V. L. Mikheev, S. P. Tret'yakova *et al.*, Fiz. Elem. Chastits At. Yadra **21**, 537 (1990) [Sov. J. Part. Nucl. **21**, 231 (1990)].
[150] J. C. Hadler, C. M. Lattes, M. Marques *et al.*, Nucl. Tracks **5**, 45 (1981).
[151] N. I. Tarantin, G. N. Buklanov, and Kim Su Men, Preprint R6-86-214 [in Russian], JINR, Dubna (1986).
[152] V. A. Nikolaev and V. P. Perelygin, Prib. Tekh. Eksp. No. 2, 7 (1976).
[153] V. A. Nikolaev, Izv. Akad. Nauk SSSR, Ser. Fiz. **35**, 180 (1971).
[154] G. M. Ter-Akop'yan, "Investigations into the synthesis and search for naturally occurring superheavy elements," Doctoral Dissertation [in Russian], JINR, Dubna (1984).
[155] G. N. Flerov, Preprint R7-11087 [in Russian], JINR, Dubna (1977).
[156] D. Lhagvasuren, V. P. Perelygin, S. G. Stetsenko *et al.*, in *Proc. of the Tenth Intern. Conf. on Solid State Nuclear Track Detectors* (Pergamon Press, Oxford, 1980), p. 939.
[157] H. A. Khan and S. A. Durrani, Nucl. Instrum. Methods **98**, 229 (1972).
[158] B. Jakupi, D. Lhagvasuren, O. Otgonsuren *et al.*, in *Proc. of the Tenth Intern. Conf. on Solid State Nuclear Track Detectors* (Pergamon Press, Oxford, 1980), p. 997.
[159] O. Otgonsuren, V. P. Perelygin, S. G. Stetsenko, Prib. Tekh. Eksp. No. 2, 49 (1977).
[160] L. Tommasino and W. G. Gross, Health Phys. **15**, 196 (1968).
[161] S. P. Tret'yakova, L. V. Jolos, and V. A. Ponomarenko, "Detection of a spontaneously fissioning nuclide in the Allende meteorite," Communication 15-83-888 [in Russian], JINR, Dubna (1983).
[162] V. P. Perelygin and S. G. Stetsenko, Pis'ma Zh. Eksp. Teor. Fiz. **32**, 622 (1980) [JETP Lett. **32**, 608 (1980)].

[163] V. P. Perelygin, S. G. Stetsenko, and O. Otgonsuren, Nucl. Tracks **12**, 375 (1986).
[164] C. Perron, M. Bourot-Denise, V. P. Perelygin *et al.*, Nucl. Tracks **15**, 231 (1988).
[165] G. B. Zhdanov, Usp. Fiz. Nauk **111**, 109 (1973) [Sov. Phys. Usp. **16**, 642 (1973)].
[166] G. N. Flerov and G. M. Ter-Akopyan, in *Treatise on Heavy-Ion Science*, edited by Bromli, Vol. 4 (Plenum Press, New York, 1985), p. 333.
[167] R. Brandt, in *Proc. of the Intern. Symposium on Superheavy Elements*, Lubbock (Pergamon Press, 1978).
[168] D. Lal, R. S. Rajan, and A. S. Tamhane, Nature **221**, 33 (1969).
[169] R. Brandt, Nucl. Instrum. Methods **173**, 111, 147 (1980).
[170] M. Debeavais and S. Trippier, Nucl. Instrum. Methods **173**, 157 (1980).
[171] V. P. Perelygin, S. P. Tretyakova, N. H. Shadieva *et al.*, in *Proc. of the First Intern. Conf. on Nuclear Tracks in Solids*, Vol. 1 (Univ. of Clermont-Ferrand Press, 1969), p. 28.
[172] V. Metag, E. Liukkonen, and G. Slettenn, Nucl. Instrum. Methods **114**, 445 (1974).
[173] N. S. Robotnov, G. N. Smirenkin, A. S. Soldatov *et al.*, in *Proc. of the First Symposium on Physics and Chemistry of Fission* (Vienna, 1966), p. 1137.
[174] H. Afarideh, S. A. Durrani, and K. Kandle, Nucl. Tracks Rad. Meas. **15**, 337 (1988).
[175] G. D. Sames and S. Graingem, Nucl. Tracks Radiat. Meas. **8**, 529 (1984).
[176] S. Huds and S. Katcoff, Phys. Rev. C **13**, 1966 (1976).
[177] O. E. Shigaev, V. S. Bychenkov, M. F. Lomanov *et al.*, Yad. Fiz. **27**, 1424 (1978) [Sov. J. Nucl. Phys. **27**, 751 (1978)].
[178] R. Brandt, F. Carbonova, E. Cieslak *et al.*, J. Phys. **31**, 21 (1970).
[179] L. Husain and S. Katkoff, Phys. Rev. C **4**, 263 (1971); **14**, 628 (1976).
[180] Z. Todorovic and R. Anatansijevic, Nuovo Cimento **34**, 545 (1976).
[181] R. Brandt, Angew. Chem. **83**, 1000 (1971).
[182] P. Vater, H. J. Becker, R. Brandt, and H. Freiesleben, Nucl. Instrum. Methods **147**, 271 (1977); Phys. Rev. Lett. **39**, 594 (1977).
[183] A. Khan, K. Rashid, A. Akber *et al.*, Nucl. Instrum. Methods **173**, 155, 163 1980).
[184] R. Brandt, A. Kapustsik, V. P. Perelygin *et al.*, in *Proc. of the Intern. Conf. on Heavy-Ion Physics*, No. 3, D7-5345 [in Russian], JINR, Dubna (1970), p. 39.
[185] V. P. Perelygin, N. H. Shadieva, S. P. Tretyakova *et al.*, Nucl. Phys. **147**, 271 (1969).
[186] P. A. Gottschalk, P. Vater, H.-J. Becker *et al.*, Phys. Rev. Lett. **42**, 359 1728 (1979).
[187] H. A. Khan, P. Vater, and R. Brandt, see Ref. 2, p. 915.
[188] M. Debeauvais, S. Jokis, and S. Tripier, see Ref. 2, p. 927.
[189] L. Todorovich, R. Anatanasijevic, and B. Grabez, see Ref. 2, p. 899.
[190] M. Debeauvais, S. Ralarosy, J. Tripier *et al.*, see Ref. 63, p. 763.
[191] M. A. Khan, R. Beckmann, P. Vater *et al.*, see Ref. 63, p. 775.
[192] M. Debeauvais, S. Ralarosy, S. Tripier *et al.*, Nucl. Tracks Radiat. Meas. **8**, 515 (1984).
[193] P. Vater, E. V. Khan, R. Beckmann *et al.*, see Ref. 192, p. 541.
[194] S. A. Karamyan, Yu. Ts. Oganesyan, and K. N. Sharifov, Yad. Fiz. **11**, 304 (1970) [Sov. J. Nucl. Phys. **11**, 170 (1970)].
[195] A. S. Il'inov, S. A. Karamyan, Nguen Tak An *et al.*, Preprint R7-6316 [in Russian], JINR, Dubna (1972).
[196] Yu. P. Gangrskiĭ, Nguen Kong Khan', At. Energ. **33**, 829 (1972).
[197] Yu. P. Gangrskiĭ, B. A. Gvozdev, B. N. Markov *et al.*, Preprint R2-769 [in Russian], JINR, Dubna (1966).
[198] R. Vandenbosch, Ann. Rev. Nucl. Sci. **27**, 1 (1977).
[199] Yu. Ts. Oganessian, M. Hussonnois, A. G. Demin *et al.*, Radiochim. Acta **37**, 113 (1984).
[200] Yu. Ts. Oganesyan, Yu. V. Lobanov, S. P. Tret'yakova *et al.*, At. Energ. **28**, 393 (1970).
[201] Yu. Ts. Oganesyan, Yu. V. Lobanov, and M. Yussonua, Preprint D7-87-392 [in Russian], JINR, Dubna (1987).
[202] Yu. Ts. Oganessian, A. G. Demin, A. S. Iljinov *et al.*, Nucl. Phys. **A239**, 157 (1975).
[203] V. A. Druin, Yu. P. Kharitonov, Yu. S. Korotkin *et al.*, Yad. Fiz. **24**, 254 (1976) [Sov. J. Nucl. Phys. **24**, 131 (1976)].
[204] A. V. Yeremin, A. N. Andreev, D. D. Bogdanov *et al.*, Nucl. Instrum. Methods **A274**, 528 (1989).
[205] I. Zvara, Yu. T. Chuburkov, T. S. Zvarova *et al.*, Radiokhimiya **11**, 154 (1969).
[206] Yu. P. Gangrskiĭ, B. N. Markov, S. M. Polikanov *et al.*, Izv. Akad. Nauk SSSR, Ser. Fiz. **32**, 1645 (1968).
[207] Yu. P. Gangrskiĭ, T. Nad', I. Vinnan *et al.*, At. Energ. **31**, 156 (1971).
[208] G. Sletten, V. Metag, and E. Liukkonen, Phys. Lett. **60B**, 153 (1976).
[209] S. A. Karamyan, Fiz. Elem. Chastits At. Yadra **17**, 753 (1986) [Sov. J. Part. Nucl. **17**, 333 (1986)].
[210] V. N. Bugrov, F. E. Epifanenkov, and S. A. Karamyan, Communication R7-88-145 [in Russian], JINR, Dubna (1988).
[211] G. D. Sames and S. Grainger, see Ref. 11, p. 529.
[212] G. D. Somogyi, I. Hunyadi, E. Koltay *et al.*, Nucl. Instrum. Methods **147**, 287 (1977).
[213] I. Hunyadi, I. M. Szoghy, and B. Cujes, see Ref. 212, p. 525.
[214] S. Szabo, Csikai, and M. Varnagy, Nucl. Phys. **A195**, 527 (1972).
[215] H. A. Khan, K. Jamil, N. A. Khan *et al.*, see Ref. 212, p. 533.
[216] H. A. Khan and I. E. Qureshi, see Ref. 26, p. 345.
[217] H. Afariden, K. Randle, S. A. Durrani *et al.*, see Ref. 84, p. 441.
[218] M. Ahmed, see Ref. 84, p. 453.
[219] I. E. Qureshi, see Ref. 84, p. 457.
[220] I. Tanihata, H. Hamagaki, O. Hashimoto *et al.*, Phys. Lett. **160B**, 380 (1985).
[221] I. Tanihata, Nucl. Phys. **A488**, 113 (1988).
[222] B. Grabez, R. Beckmann, P. Vater *et al.*, Phys. Rev. C **34**, 170 (1986); Phys. Lett. **184B**, 144 (1987).
[223] H. A. Khan, T. Lund, P. Vater, and R. Brandt, Phys. Rev. C **28**, 1630 (1983); **32**, 1551 (1985).
[224] H. A. Khan, N. A. Khan, and M. Ahmad, Nucl. Instrum. Methods **B23**, 359 (1987).
[225] M. Zamani, M. Debeauvais, S. Ralarasy *et al.*, Phys. Rev. C **42**, 331 (1990).
[226] W. Heinrich, C. Brechtmann, S. Dreute, and D. Weidmann, see Ref. 84, p. 393.
[227] H. A. Khan, I. E. Qureshi, K. Jamil *et al.*, see Ref. 84, p. 403.
[228] I. E. Qureshi, see Ref. 84, p. 411; Nucl. Phys. **A477**, 510 (1988).
[229] I. E. Qureshi and H. A. Khan, see Ref. 84, p. 423.
[230] Bhattacharyya, A. K. Ganguly, and I. Hunyadij, Nucl. Instrum. Methods **B47**, 466 (1990).
[231] B. Crabez, P. Vater, and R. Brandt, Nucl. Instrum. Methods **B42**, 286 (1989).
[232] J. D. Stevenson and P. B. Price, Phys. Rev. C **24**, 2102 (1981).
[233] P. B. Price and M. H. Salamon, see Ref. 26, p. 5.
[234] J. H. Chan and P. B. Price, Phys. Rev. Lett. **35**, 539 (1975).
[235] P. H. Fowler, C. Alexandre, V. M. Claphan *et al.*, Nucl. Instrum. Methods **147**, 195 (1977).
[236] N. L. Grigorov, V. V. Bobrovskaya, M. A. Kondrat'eva *et al.*, Preprint 88-48/68 [in Russian], Institute of Nuclear Physics, Moscow State University (1988).
[237] Yu. F. Gagarin, Ya. B. Dvoryanchikov, and V. M. Megulin, Preprint No. 1430 [in Russian], A. F. Ioffe Physicotechnical Institute, Leningrad (1990).
[238] W. Enge, Nucl. Instrum. Methods **147**, 211 (1977).
[239] K. Ocura, S. Orito, S. Nakamura *et al.*, Nucl. Tracks Rad. Meas. **16**, 107 (1989).
[240] Yu. A. Shukolyukov, *Fission of Uranium Nuclei in Nature* [in Russian] (Atomizdat, Moscow, 1970).
[241] G. N. Flerov and I. G. Berzina, *Radiography of Minerals, Rocks, and Ores* [in Russian] (Atomizdat, Moscow, 1979).
[242] Yu. F. Babikova, A. A. Gusakov, V. N. Minaev, and G. G. Ryabova, *Analytic Autoradiography* [in Russian] (Énergoatomizdat, Moscow, 1985).
[243] L. Tommasino and R. V. Griffith, *The Dosimetry of Ionizing Radiation*, Vol. 3 (Academic Press, Rome, 1990).
[244] G. N. Flerov, Vestn. Akad. Nauk SSSR No. 4, 35 (1984).
[245] *Proc. of the Intern. Workshop on Radon Monitoring in Radioprotection, Environmental Radioactivity and Earth Sciences*, ICTP, Trieste, Italy, 1989, edited by L. Tommasino, G. Furlan, N. A. Khan, and M. Monin (World Scientific, Singapore, 1990).

Translated by Julian B. Barbour